

CITATION REPORT

List of articles citing

Reproducibility in density functional theory calculations of solids

DOI: 10.1126/science.aad3000
Science, 2016, 351, aad3000.

Source: <https://exaly.com/paper-pdf/65442748/citation-report.pdf>

Version: 2024-04-28

This report has been generated based on the citations recorded by exaly.com for the above article. For the latest version of this publication list, visit the link given above.

The third column is the impact factor (IF) of the journal, and the fourth column is the number of citations of the article.

#	Paper	IF	Citations
964	Obituary for Walter Kohn (1923-2016). 2016 , 4, 40		1
963	Photocatalytic Water Splitting-The Untamed Dream: A Review of Recent Advances. 2016 , 21,		359
962	Lattice thermal expansion and anisotropic displacements in α -sulfur from diffraction experiments and first-principles theory. 2016 , 145, 234512		17
961	Modeling Dilute Solutions Using First-Principles Molecular Dynamics: Computing more than a Million Atoms with over a Million Cores. 2016 ,		10
960	Stable isomers and electronic, vibrational, and optical properties of WS nano-clusters: A first-principles study. 2016 , 145, 214303		5
959	First-principles investigation of the structural, dynamical, and dielectric properties of kesterite, stannite, and PMCA phases of $\text{Cu}_2\text{ZnSnS}_4$. 2016 , 94,		18
958	Tree based machine learning framework for predicting ground state energies of molecules. 2016 , 145, 134101		14
957	Error estimates for density-functional theory predictions of surface energy and work function. 2016 , 94,		71
956	Perspective: Kohn-Sham density functional theory descending a staircase. 2016 , 145, 130901		186
955	Trends for isolated amino acids and dipeptides: Conformation, divalent ion binding, and remarkable similarity of binding to calcium and lead. 2016 , 6, 35772		18
954	Extension of the basis set of linearized augmented plane wave (LAPW) method by using supplemented tight binding basis functions. 2016 , 145, 014101		9
953	Toward Routine Gauge-Including Projector Augmented-Wave Calculations for Metallic Systems: The Case of ScT_2Al (T = Ni, Pd, Pt, Cu, Ag, Au) Heusler Phases. 2016 , 120, 25530-25540		6
952	Is the error on first-principles volume predictions absolute or relative?. 2016 , 117, 390-396		13
951	Combining solid-state NMR spectroscopy with first-principles calculations - a guide to NMR crystallography. 2016 , 52, 7186-204		164
950	Single-Layered Hittorf's Phosphorus: A Wide-Bandgap High Mobility 2D Material. 2016 , 16, 2975-80		153
949	On the crystalline structure of orthorhombic SrRuO_3 : A benchmark study of DFT functionals. 2016 , 124, 78-86		4
948	Precision of Electric-Field Gradient Predictions by Density Functional Theory and Implications for the Nuclear Quadrupole Moment and Its Error Bar of the ^{111}Cd 245 keV $5/2^+$ Level. 2016 , 120, 23111-23120		19

947	Highly Efficient Free Energy Calculations of the Fe Equation of State Using Temperature-Dependent Effective Potential Method. 2016 , 120, 8761-8768	5
946	Big data need big theory too. 2016 , 374,	103
945	Applications of large-scale density functional theory in biology. 2016 , 28, 393001	81
944	Liquid Water through Density-Functional Molecular Dynamics: Plane-Wave vs Atomic-Orbital Basis Sets. 2016 , 12, 3456-62	19
943	Evaluating the size of Fe nanoparticles for ammonia adsorption and dehydrogenation. 2016 , 124, 220-227	9
942	Computational Screening of All Stoichiometric Inorganic Materials. 2016 , 1, 617-627	72
941	Pressure induced elastic softening in framework aluminosilicate- albite (NaAlSiO). 2016 , 6, 34815	15
940	Modelling the structure of Zr-rich Pb(ZrTi)O, $x = 0.4$ by a multiphase approach. 2016 , 18, 28316-28324	8
939	Landau levels in 2D materials using Wannier Hamiltonians obtained by first principles. 2016 , 3, 035023	15
938	Deleterious Effects of Exact Exchange Functionals on Predictions of Molecular Conductance. 2016 , 12, 3431-5	7
937	Physical properties of the Ce ₂ MAI ₇ Ge ₄ heavy-fermion compounds (M=Co,Ir,Ni,Pd). 2016 , 93,	3
936	Nonlinear elastic effects in phase field crystal and amplitude equations: Comparison to ab initio simulations of bcc metals and graphene. 2016 , 93,	14
935	First-principles studies of the Gilbert damping and exchange interactions for half-metallic Heuslers alloys. 2016 , 93,	16
934	High photon energy spectroscopy of NiO: Experiment and theory. 2016 , 93,	15
933	Sustainable Nanotechnology: Opportunities and Challenges for Theoretical/Computational Studies. 2016 , 120, 7297-306	42
932	Magnetovolume effect, macroscopic hysteresis, and moment collapse in the paramagnetic state of cubic MnGe under pressure. 2016 , 93,	16
931	Making the most of materials computations. <i>Science</i> , 2016 , 354, 180-181	33:3 27
930	Performance of DFT+U Approaches in the Study of Catalytic Materials. 2016 , 6, 8370-8379	99

929	A DFT study of the effect of SO groups on the properties of TiO nanoparticles. 2016 , 18, 33068-33076	6
928	Assessing the influence of van der Waals corrected exchange-correlation functionals on the anisotropic mechanical properties of coinage metals. 2016 , 94,	13
927	Noncovalent Bonding Controls Selectivity in Heterogeneous Catalysis: Coupling Reactions on Gold. 2016 , 138, 15243-15250	35
926	Magnetocrystalline anisotropy of FePt: A detailed view. 2016 , 94,	29
925	Implementation of Constrained DFT for Computing Charge Transfer Rates within the Projector Augmented Wave Method. 2016 , 12, 5367-5378	38
924	The role of ionic sizes in inducing the cubic to tetragonal distortion in AV_2O_4 and ACr_2O_4 (A= Zn, Mg and Cd) compounds. 2016 , 3, 116301	1
923	Functional Independent Scaling Relation for ORR/OER Catalysts. 2016 , 120, 24910-24916	86
922	BaCu ₂ Sn(S,Se) ₄ : Earth-Abundant Chalcogenides for Thin-Film Photovoltaics. 2016 , 28, 4771-4780	101
921	PHYSICS. A benchmark for materials simulation. <i>Science</i> , 2016 , 351, 1394-5	33-3 17
920	First principle study on water protons interacted with gadolinium oxide and gold nanocluster. 2017 , 667, 91-95	2
919	A New Type of Scaling Relations to Assess the Accuracy of Computational Predictions of Catalytic Activities Applied to the Oxygen Evolution Reaction. 2017 , 9, 1261-1268	61
918	A computational framework for automation of point defect calculations. 2017 , 130, 1-9	83
917	Pressure effect on the mechanical, electronic and thermodynamic properties of Ba ₂ Bi ₃ : First-principle calculations. 2017 , 104, 293-303	5
916	Molecular and Electronic Structures of MO (M = Mn, Tc, Re). 2017 , 56, 2448-2458	13
915	Solubility of argon in laser additive manufactured titanium under hot isostatic pressing condition. 2017 , 131, 209-219	41
914	Finite-strain Landau theory applied to the high-pressure phase transition of lead titanate. 2017 , 95,	10
913	Alternative structure of TiO ₂ with higher energy valence band edge. 2017 , 95,	7
912	Elucidation of the helical spin structure of FeAs. 2017 , 95,	6

911	Towards an accurate description of perovskite ferroelectrics: exchange and correlation effects. 2017 , 7, 43482	36
910	First-principles study of paraelectric and ferroelectric CsH ₂ PO ₄ including dispersion forces: Stability and related vibrational, dielectric, and elastic properties. 2017 , 95,	11
909	Thermodynamics of the Flexible Metal-Organic Framework Material MIL-53(Cr) From First Principles. 2017 , 121, 4312-4317	29
908	Tuning the electronic and vibrational properties of SnPSe and PbPS crystals and their metallization under high pressure. 2017 , 46, 4245-4258	13
907	First-Principles Modeling of Point Defects and Complexes in Thin-Film Solar-Cell Absorber CuInSe ₂ . 2017 , 3, 1600353	24
906	Reproducible Research in Computational Chemistry of Materials. 2017 , 29, 2615-2617	18
905	Chemical misfit origin of solute strengthening in iron alloys. 2017 , 131, 445-456	21
904	Prospects of spintronics based on 2D materials. 2017 , 7, e1313	105
903	Charge Transport in Nanostructured Materials: Implementation and Verification of Constrained Density Functional Theory. 2017 , 13, 2581-2590	27
902	The electronic band structure of Ge _{1-x} Sn _x in the full composition range: indirect, direct, and inverted gaps regimes, band offsets, and the Burstein-Moss effect. 2017 , 50, 195103	52
901	Investigating Sodium Storage Mechanisms in Tin Anodes: A Combined Pair Distribution Function Analysis, Density Functional Theory, and Solid-State NMR Approach. 2017 , 139, 7273-7286	86
900	Benchmarking Quantum Chemical Methods: Are We Heading in the Right Direction?. 2017 , 56, 11011-11018	90
899	Software Platforms for Electronic/Atomistic/Mesosopic Modeling: Status and Perspectives. 2017 , 6, 92-110	4
898	Thermodynamic Equilibria in Carbon Nitride Photocatalyst Materials and Conditions for the Existence of Graphitic Carbon Nitride g-C ₃ N ₄ . 2017 , 29, 4445-4453	38
897	Uncertainties in Theoretical Description of Well-Defined Heterogeneous Catalysts. 2017 , 177, 541-565	1
896	Quantum and isotope effects in lithium metal. <i>Science</i> , 2017 , 356, 1254-1259	33-3 38
895	Modeling resistive switching materials and devices across scales. 2017 , 39, 39-60	11
894	Excellent Thermoelectric Performance Predicted in Two-Dimensional Buckled Antimonene: A First-Principles Study. 2017 , 121, 13035-13042	55

893	Parity-Forbidden Transitions and Their Impact on the Optical Absorption Properties of Lead-Free Metal Halide Perovskites and Double Perovskites. 2017 , 8, 2999-3007	267
892	Concentration effect on equilibrium fractionation of Mg-Ca isotopes in carbonate minerals: Insights from first-principles calculations. 2017 , 208, 185-197	48
891	Unraveling Thermodynamics, Stability, and Oxygen Evolution Activity of Strontium Ruthenium Perovskite Oxide. 2017 , 7, 3245-3256	74
890	Absolute Binding Energies of Core Levels in Solids from First Principles. 2017 , 118, 026401	30
889	Opinion: Quantum solutions for a sustainable energy future. 2017 , 1,	12
888	CC/BN substitution in five membered heterocycles. A computational analysis. 2017 , 41, 3619-3633	8
887	Insight into the local environment of magnesium and calcium in low-coordination-number organo-complexes using Mg and Ca solid-state NMR: a DFT study. 2017 , 73, 208-218	4
886	Missing Linkers: An Alternative Pathway to UiO-66 Electronic Structure Engineering. 2017 , 29, 3006-3019	120
885	Dirac's dream: Understanding metal sorption by geomedia using density functional theory. 2017 , 464, 4-13	12
884	The Elephant in the Room of Density Functional Theory Calculations. 2017 , 8, 1449-1457	60
883	ALMB (M = Cr, Mn, Fe, Co, Ni): a group of nanolaminated materials. 2017 , 29, 155402	44
882	Interfacial engineering of phthalocyanine molecules on graphitic and metal substrates. 2017 , 43, 384-393	2
881	Interactions of calcium with the external surfaces of fullerenes and endofullerenes doped with radioactive sodium iodide. 2017 , 23, 15	2
880	Well-defined linear Au (n = 2-4) chains encapsulated in SWCNTs: a DFT study. 2017 , 23, 19	
879	Molecular Crystal Engineering: Tuning Organic Semiconductor from p-type to n-type by Adjusting Their Substitutional Symmetry. 2017 , 29, 1605053	47
878	High-Throughput Screening of Extrinsic Point Defect Properties in Si and Ge: Database and Applications. 2017 , 29, 975-984	7
877	A local Fock-exchange potential in Kohn-Sham equations. 2017 , 29, 04LT01	10
876	Role of Point Defects in Spinel Mg Chalcogenide Conductors. 2017 , 29, 9657-9667	34

875	High-throughput DFT calculations of formation energy, stability and oxygen vacancy formation energy of ABO perovskites. 2017 , 4, 170153	144
874	Implications of the DFT+U method on polaron properties in energy materials. 2017 , 96,	22
873	Characteristics of lithium adsorption near divacancy defects on carbon nanotubes (7,7). 2017 , 79, 127-132	4
872	Ab initio random structure searching of organic molecular solids: assessment and validation against experimental data. 2017 , 19, 25949-25960	13
871	Advanced capabilities for materials modelling with Quantum ESPRESSO. 2017 , 29, 465901	2275
870	A series of sulfonic acid functionalized mixed-linker DUT-4 analogues: synthesis, gas sorption properties and catalytic performance. 2017 , 46, 14356-14364	10
869	$IVVI$ ($I = Cu, Ag; II = Sr, Ba; IV = Ge, Sn; VI = S, Se$): Chalcogenides for Thin-Film Photovoltaics. 2017 , 29, 7868-7879	67
868	Round Robin Study: Molecular Simulation of Thermodynamic Properties from Models with Internal Degrees of Freedom. 2017 , 13, 4270-4280	32
867	Auxiliary-field quantum Monte Carlo calculations with multiple-projector pseudopotentials. 2017 , 95,	16
866	Exchange constants in molecule-based magnets derived from density functional methods. 2017 , 96,	6
865	Effect of Ca content on equilibrium Ca isotope fractionation between orthopyroxene and clinopyroxene. 2017 , 219, 44-56	41
864	Prediction of the stability of the rhombohedral phase in $IVVI$ monochalcogenides and its origin. 2017 , 19, 6107-6115	10
863	Revealing and exploiting hierarchical material structure through complex atomic networks. 2017 , 3,	16
862	Latent Porosity in Alkali-Metal MBF Salts: Structures and Rapid Room-Temperature Hydration/Dehydration Cycles. 2017 , 56, 12023-12041	9
861	Pseudopotential for electronic structure calculations of uranium compounds. 2017 , 38, 974-977	5
860	Evaluation of thermodynamics, formation energetics and electronic properties of vacancy defects in CaZrO. 2017 , 7, 8439	24
859	High-throughput Identification and Characterization of Two-dimensional Materials using Density functional theory. 2017 , 7, 5179	122
858	Plane-wave pseudopotential implementation and performance of SCAN meta-GGA exchange-correlation functional for extended systems. 2017 , 146, 224105	34

- 857 Influence of the Exchange-Correlation Functional on the Energy of Formation and Magnetic Behavior of Binary D03 Intermetallic Compounds FeM₃ (M = Ti, Zr, Hf). **2017**, 38, 231-237
- 856 Quantenchemische Methoden im Leistungsvergleich: Stimmt die Richtung noch?. **2017**, 129, 11155-11163 11
- 855 Modelling pH and potential in dynamic structures of the water/Pt(111) interface on the atomic scale. **2017**, 19, 23505-23514 40
- 854 Effect of pressure on structural, elastic and mechanical properties of transition metal hydrides Mg₇TMH₁₆ (TM = Sc, Ti, V, Y, Zr and Nb): First-principles investigation. **2017**, 111, 229-237 3
- 853 Toward high value sensing: monolayer-protected metal nanoparticles in multivariable gas and vapor sensors. **2017**, 46, 5311-5346 55
- 852 Atomistic spin dynamics simulations of the MnAl ϵ phase and its antiphase boundary. **2017**, 96, 14
- 851 First-Principles Study of Alkoxides Adsorbed on Au(111) and Au(110) Surfaces: Assessing the Roles of Noncovalent Interactions and Molecular Structures in Catalysis. **2017**, 121, 27905-27914 10
- 850 Assessing the performance of self-consistent hybrid functional for band gap calculation in oxide semiconductors. **2017**, 29, 454004 27
- 849 Hydrogen accumulation around dislocation loops and edge dislocations: from atomistic to mesoscopic scales in BCC tungsten. **2017**, T170, 014073 9
- 848 Efficient Construction of Free Energy Profiles of Breathing Metal-Organic Frameworks Using Advanced Molecular Dynamics Simulations. **2017**, 13, 5861-5873 33
- 847 The cohesive energy of superheavy element copernicium determined from accurate relativistic coupled-cluster theory. **2017**, 19, 32286-32295 13
- 846 Applications of Solid-State ⁴³Ca Nuclear Magnetic Resonance: Superconductors, Glasses, Biomaterials, and NMR Crystallography. **2017**, 92, 227-363 7
- 845 Ab Initio Investigation of the Role of CO Adsorption on the Physical Properties of 55-Atom PtCo Nanoalloys. **2017**, 121, 27721-27732 9
- 844 Towards efficient data exchange and sharing for big-data driven materials science: metadata and data formats. **2017**, 3, 53
- 843 Automation methodologies and large-scale validation for GW: Towards high-throughput GW calculations. **2017**, 96, 31
- 842 First-principles calculations of tetragonal FeX (X= S, Se, Te): Magnetism, hyperfine-interaction, and bonding. **2017**, 441, 769-775 1
- 841 Finite-temperature properties of nonmagnetic transition metals: Comparison of the performance of constraint-based semilocal and nonlocal functionals. **2017**, 95, 32
- 840 Evolutionary optimization of PAW data-sets for accurate high pressure simulations. **2017**, 347, 39-55 5

839	Precipitation in simultaneously nitrated and aged Mo-containing maraging steel. 2017 , 131, 21-30	8
838	Robustness of the quantum spin Hall insulator phase in monolayer 1T' transition metal dichalcogenides. 2017 , 219, 72-76	7
837	Challenges in large scale quantum mechanical calculations. 2017 , 7, e1290	65
836	Atomistic calculations and materials informatics: A review. 2017 , 21, 167-176	122
835	Computational Chemistry Methods for Nanoporous Materials. 2017 , 29, 199-212	54
834	Review of two-dimensional materials for photocatalytic water splitting from a theoretical perspective. 2017 , 7, 545-559	251
833	Linear-scaling density functional theory using the projector augmented wave method. 2017 , 29, 024001	10
832	Entropic contributions enhance polarity compensation for CeO(100) surfaces. 2017 , 16, 328-334	57
831	Hydrogen Treatment as a Detergent of Electronic Trap States in Lead Chalcogenide Nanoparticles. 2017 , 29, 2485-2493	14
830	A new generation of effective core potentials for correlated calculations. 2017 , 147, 224106	46
829	Accuracy and Transferability of Ab Initio Electronic Band Structure Calculations for Doped BiFeO ₃ . 2017 , 921, 012009	3
828	Visualising crystal packing interactions in solid-state NMR: Concepts and applications. 2017 , 147, 144203	15
827	Ab initio study of magnetocrystalline anisotropy, magnetostriction, and Fermi surface of L10FeNi (tetraenaite). 2017 , 50, 495008	11
826	Neutron total cross section calculation within the framework of quasi-harmonic approximation. 2017 , 19, 103027	2
825	Doping LiMnPO ₄ with Cobalt and Nickel: A First Principle Study. 2017 , 3, 11	11
824	Insertion of Mono- vs. Bi- vs. Trivalent Atoms in Prospective Active Electrode Materials for Electrochemical Batteries: An ab Initio Perspective. 2017 , 10, 2061	7
823	Organic materials database: An open-access online database for data mining. 2017 , 12, e0171501	34
822	Challenges for Theory and Computation. 2017 , 5, 49	1

821	Validation of missed space-group symmetry in X-ray powder diffraction structures with dispersion-corrected density functional theory. 2017 , 73, 756-766	1
820	Prediction of site occupancy of C15 Laves phase at finite temperature based on quasi-harmonic approximation model. 2018 , 96, 33-40	6
819	Characterization of point defects in monolayer arsenene. 2018 , 443, 74-82	26
818	A high-throughput exploration of magnetic materials by using structure predicting methods. 2018 , 123, 083904	6
817	Quantum Crystallography: Current Developments and Future Perspectives. 2018 , 24, 10881-10905	77
816	Reactive Dynamics Simulation Study on the Pyrolysis of Polymer Precursors To Generate Amorphous Silicon Oxycarbide Structures. 2018 , 122, 5767-5773	6
815	The PseudoDojo: Training and grading a 85 element optimized norm-conserving pseudopotential table. 2018 , 226, 39-54	473
814	Structural, electronic and optical properties of LiNbO3 using GGA-PBE and TB-mBJ functionals: A DFT study. 2018 , 32, 1850168	14
813	Exploring Lanthanide Doping in UiO-66: A Combined Experimental and Computational Study of the Electronic Structure. 2018 , 57, 5463-5474	34
812	Microhartree precision in density functional theory calculations. 2018 , 97,	14
811	Fluorographane C2FH: Stable and wide band gap insulator with huge excitonic effect. 2018 , 135, 134-144	12
810	First-Principles Statistical Mechanics of Multicomponent Crystals. 2018 , 48, 27-55	61
809	Implications of bond disorder in a S=1 kagome lattice. 2018 , 8, 4745	3
808	Quantum diffusion of H/D on Ni(111)-A partially adiabatic centroid MD study. 2018 , 148, 102339	3
807	Local spin structure of the RuCl3 honeycomb-lattice magnet observed via muon spin rotation/relaxation. 2018 , 97,	5
806	Ab initio Eliashberg Theory: Making Genuine Predictions of Superconducting Features. 2018 , 87, 041012	40
805	Tracking the ultrafast XUV optical properties of x-ray free-electron-laser heated matter with high-order harmonics. 2018 , 97,	13
804	Label-free surface plasmon resonance biosensing with titanium nitride thin film. 2018 , 106, 129-135	12

803	GW100: Comparison of Methods and Accuracy of Results Obtained with the WEST Code. 2018 , 14, 1895-1909	41
802	Two-dimensional materials from high-throughput computational exfoliation of experimentally known compounds. 2018 , 13, 246-252	874
801	PyCDT: A Python toolkit for modeling point defects in semiconductors and insulators. 2018 , 226, 165-179	86
800	Two-dimensional MoS ₂ electromechanical actuators. 2018 , 51, 075306	34
799	LiCsLa(BO) and LiKLa(BO): new mixed alkali metal lanthanum borates with three-dimensional open frameworks and short cut-off edges. 2018 , 47, 3512-3520	4
798	Effect of Basicity on the Hydrolysis of the Bi(III) Aqua Ion in Solution: An Ab Initio Molecular Dynamics Study. 2018 , 122, 1905-1915	11
797	Benchmark Database of Transition Metal Surface and Adsorption Energies from Many-Body Perturbation Theory. 2018 , 122, 4381-4390	32
796	Energy Level Alignment at Interfaces Between Au (111) and Thiolated Oligophenylenes of Increasing Chain Size: Theoretical Evidence of Pinning Effects. 2018 , 1, 1700020	10
795	Affordable and accurate large-scale hybrid-functional calculations on GPU-accelerated supercomputers. 2018 , 30, 095901	7
794	Intramolecular BSSE and dispersion affect the structure of a dipeptide conformer. 2018 , 116, 1236-1244	4
793	Polymorph transitions in uranium at low temperatures: first-principles investigation. 2018 , 26, 025009	3
792	Nuclear quantum effects of light and heavy water studied by all-electron first principles path integral simulations. 2018 , 148, 102324	13
791	NaCl-CsCl structural transition in Sr ₂ PdO ₃ and Sr ₂ TiO ₄ . 2018 , 737, 230-237	1
790	Ab initio study on the structural and electronic properties of water surrounding a multifunctional nanoprobe. 2018 , 530, 69-74	1
789	Computational insight into magnetic behavior and properties of the transition metal complexes with redox-active ligands: a DFT approach. 2018 , 90, 811-824	27
788	Phase Diagram of Hydrogen and a Hydrogen-Helium Mixture at Planetary Conditions by Quantum Monte Carlo Simulations. 2018 , 120, 025701	54
787	Comparison of the Performance of van der Waals Dispersion Functionals in the Description of Water and Ethanol on Transition Metal Surfaces. 2018 , 122, 1577-1588	25
786	Ab Initio Study of the Electronic Structure, Elastic Properties, Magnetic Feature and Thermodynamic Properties of the Ba ₂ NiMoO ₆ Material. 2018 , 192, 265-285	10

785	High-throughput density-functional perturbation theory phonons for inorganic materials. 2018 , 5, 180065	75
784	Electron-phonon interaction and superconductivity in representative AuCu ₃ -type intermetallic compounds. 2018 , 150, 491-499	5
783	Thermodynamically accessible titanium clusters Ti _N , N = 2-32. 2018 , 20, 13962-13973	10
782	Thermodynamic limit for synthesis of metastable inorganic materials. 2018 , 4, eaaq0148	106
781	Towards predictive many-body calculations of phonon-limited carrier mobilities in semiconductors. 2018 , 97,	128
780	Magnetic phase transition induced by electrostatic gating in two-dimensional square metal-organic frameworks. 2018 , 97,	4
779	The psml format and library for norm-conserving pseudopotential data curation and interoperability. 2018 , 227, 51-71	14
778	Effect of tetravalent dopants on hematite nanostructure for enhanced photoelectrochemical water splitting. 2018 , 427, 1203-1212	36
777	Recent developments in libxc [A comprehensive library of functionals for density functional theory. 2018 , 7, 1-5	180
776	Structural and electronic properties of M-MOF-74 (M = Mg, Co or Mn). 2018 , 691, 283-290	33
775	Stable structures of exohedrally decorated C ₆₀ -fullerenes. 2018 , 129, 847-853	23
774	High-pressure Raman spectra and DFT calculations of L-tyrosine hydrochloride crystal. 2018 , 531, 35-44	5
773	Phase-Field Modelling in Extractive Metallurgy. 2018 , 43, 417-454	6
772	High-Throughput Computing for Accelerated Materials Discovery. 2018 , 169-191	1
771	Building bridges: matching density functional theory with experiment. 2018 , 59, 377-390	
770	Precision and efficiency in solid-state pseudopotential calculations. 2018 , 4,	181
769	Hole transport in selenium semiconductors using density functional theory and bulk Monte Carlo. 2018 , 124, 235102	9
768	Charge-induced electromechanical actuation of Mo- and W-dichalcogenide monolayers.. 2018 , 8, 38667-38672	10

767	Influence of Crystal Structure and 3d Impurities on the Electronic Structure of the Topological Material Cd ₃ As ₂ . 2018 , 54, 1093-1098	9
766	Heterogeneous reactions of SO on the hematite(0001) surface. 2018 , 149, 194703	6
765	Tuning the balance between dispersion and entropy to design temperature-responsive flexible metal-organic frameworks. 2018 , 9, 4899	65
764	Accuracy of Partial Core Corrections Using Fourier Transforms in Pseudopotential-Density Functional Theory. 2018 , 14, 6515-6520	
763	Electronic Structure of Oxide Ultrathin Layers on Metal Surfaces. 2018 , 86-96	
762	Formation of Occupied and Unoccupied Hybrid Bands at Interfaces between Metals and Organic Donors/Acceptors. 2018 , 122, 27554-27560	8
761	Are dispersion corrections accurate outside equilibrium? A case study on benzene. 2018 , 14, 1181-1191	10
760	Efficient O(N) divide-conquer method with localized single-particle natural orbitals. 2018 , 98,	1
759	Machine Learning a General-Purpose Interatomic Potential for Silicon. 2018 , 8,	122
758	Towards simulation at picometer-scale resolution: Revisiting inversion domain boundaries in GaN. 2018 , 98,	5
757	Influence of Oxygen Vacancy Density on the Polaronic Configuration in Rutile. 2018 , 11,	5
756	Electronic Structure of Atomically Precise Graphene Nanoribbons. 2018 , 1-35	1
755	Structure Sensitivity of Formic Acid Electrooxidation on Transition Metal Surfaces: A First-Principles Study. 2018 , 165, J3109-J3121	24
754	Quantum mechanical studies of full-shell noble metal nanoclusters in water. 2018 , 118, e25709	
753	Deciphering the origin of nonlocal resistance in multiterminal graphene on hexagonal-boron-nitride with ab initio quantum transport: Fermi surface edge currents rather than Fermi sea topological valley currents. 2018 , 1, 015006	14
752	The Materials Project: Accelerating Materials Design Through Theory-Driven Data and Tools. 2018 , 1-34	7
751	Trivacancy and Stone-Wales defected silicene for adsorption of small gas molecules. 2018 , 154, 276-283	7
750	Benchmarking the performance of plane-wave vs. localized orbital basis set methods in DFT modeling of metal surface: a case study for Fe-(110). 2018 , 29, 163-167	4

749	Excitonic States in Semiconducting Two-Dimensional Perovskites. 2018 , 1, 6361-6367	19
748	Tailoring Bond Topologies in Open-Shell Graphene Nanostructures. 2018 , 12, 11917-11927	69
747	Insights on the Alumina/Water Interface Structure by Direct Comparison of Density Functional Simulations with X-ray Reflectivity. 2018 , 122, 26934-26944	16
746	Novel Methodologies to Model Charge Transport in Metal/Air Batteries. 2018 , 331-365	
745	The role of computational results databases in accelerating the discovery of catalysts. 2018 , 1, 809-810	32
744	Accuracy of theoretical catalysis from a model of iron-catalyzed ammonia synthesis. 2018 , 1,	11
743	Novel Solar Cell Materials: Insights from First-Principles. 2018 , 122, 27107-27126	19
742	First-Principles and Thermodynamics Study of Compositionally Tuned Complex Metal Oxides: Cation Release from the (001) Surface of Mn-Rich Lithium Nickel Manganese Cobalt Oxide. 2018 , 57, 13300-13311	20
741	Doping of BiFeO ₃ : A comprehensive study on substitutional doping. 2018 , 98,	36
740	Modeling the Adsorption of NO and NH ₃ on Fe-SSZ-13 from First-Principles: A DFT Study. 2018 , 57, 13396-13405	5
739	Crosslinking chemistry of poly(vinylmethyl-co-methyl)silazanes toward low-temperature formable preceramic polymers as precursors of functional aluminium-modified Si-C-N ceramics. 2018 , 47, 14580-14593	14
738	Encyclopedia of Big Data Technologies. 2018 , 1-8	1
737	Machine learning material properties from the periodic table using convolutional neural networks. 2018 , 9, 8426-8432	48
736	Assessing Density-Functional Theory for Equation-Of-State. 2018 , 6, 13	11
735	NOMAD: The FAIR concept for big data-driven materials science. 2018 , 43, 676-682	155
734	Contribution of Density Functional Theory to Microporous Materials for Carbon Capture. 2018 , 319-343	2
733	Performance of various density-functional approximations for cohesive properties of 64 bulk solids. 2018 , 20, 063020	110
732	Psi4NumPy: An Interactive Quantum Chemistry Programming Environment for Reference Implementations and Rapid Development. 2018 , 14, 3504-3511	72

731	Machine Learning and Energy Minimization Approaches for Crystal Structure Predictions: A Review and New Horizons. 2018 , 30, 3601-3612	83
730	EPAW-1.0 code for evolutionary optimization of PAW datasets especially for high-pressure applications. 2018 , 233, 110-122	0
729	Uncertainties in the predictions of thermo-physical properties of thermoplastic polymers via molecular dynamics. 2018 , 26, 065007	11
728	Covalency is Frustrating: LaSnO and the Nature of Bonding in Pyrochlores under High Pressure-Temperature Conditions. 2018 , 57, 15051-15061	9
727	Anomalous screening of an electrostatic field at the surface of niobium nitride. 2018 , 461, 17-22	10
726	PASTA: Python Algorithms for Searching Transition stAtes. 2018 , 233, 261-268	3
725	Machine learning for molecular and materials science. 2018 , 559, 547-555	1282
724	Dynamical Mean Field Theory for Oxide Heterostructures. 2018 , 215-243	
723	Evaluation of thermodynamic equations of state across chemistry and structure in the materials project. 2018 , 4,	9
722	Band gap evolution of bulk Cu ₃ N and monolayer Cu ₂ N under nonhydrostatic strain. 2018 , 266, 161-165	8
721	Dissolution Profile Consideration in Pharmaceutical Product Development. 2018 , 287-336	1
720	Structural evolution of gypsum under high pressure: single-crystal X-ray experiments revisited. 2018 , 45, 895-906	2
719	A new ab initio equation of state of hcp-Fe and its implication on the interior structure and mass-radius relations of rocky super-Earths. 2018 , 313, 61-78	38
718	The Computational 2D Materials Database: high-throughput modeling and discovery of atomically thin crystals. 2018 , 5, 042002	399
717	Carrier Lifetimes and Polaronic Mass Enhancement in the Hybrid Halide Perovskite CH ₃ NH ₃ PbI ₃ from Multiphonon Fröhlich Coupling. 2018 , 121, 086402	48
716	Observation of topologically protected states at crystalline phase boundaries in single-layer WSe. 2018 , 9, 3401	68
715	Magnetic phases of skyrmion-hosting GaV ₄ S ₈ Se _y (y=0,2,4,8) probed with muon spectroscopy. 2018 , 98,	12
714	Conducting Behavior of Crystalline PbO ₂ as Revealed by DFT Calculations. 2018 , 21,	3

713	Density Functional Theory Study of Arsenate Adsorption onto Alumina Surfaces. 2018 , 8, 91	15
712	Potential-induced nanoclustering of metallic catalysts during electrochemical CO reduction. 2018 , 9, 3117	163
711	Magnetism of new metastable cobalt-nitride compounds. 2018 , 10, 13011-13021	20
710	Design and exploration of semiconductors from first principles: A review of recent advances. 2018 , 11, 060101	70
709	A polynomial Ansatz for norm-conserving pseudopotentials. 2018 , 30, 275501	
708	Lattice dynamics and metastability of fcc metals in the hcp structure and the crucial role of spin-orbit coupling in platinum. 2018 , 97,	11
707	Predicting synthesizability. 2019 , 52,	161
706	Emergence of superconductivity in a Dirac nodal-line Cu ₂ Si monolayer: ab initio calculations. 2019 , 7, 10926-10932	13
705	Substrate strain and doping effects on the crystal structure of SrNb _x Ti _{1-x} O ₃ . 2019 , 92, 1	1
704	Brownmillerite-Type SrScGaO Oxide Ion Conductor: Local Structure, Phase Transition, and Dynamics. 2019 , 31, 7395-7404	5
703	Effects of bromine substitution for iodine on structural stability and phase transition of CsPbI ₃ . 2019 , 496, 143593	6
702	Enhancing the interfacial thermal conduction of the graphene sheets via chemical bond-bond connections. 2019 , 9, 085106	
701	Alternative approach to populate and study the Th ²²⁹ nuclear clock isomer. 2019 , 100,	8
700	Electrochemical stability and light-harvesting ability of silicon photoelectrodes in aqueous environments. 2019 , 151, 044109	2
699	Adsorption on transition metal surfaces: Transferability and accuracy of DFT using the ADS41 dataset. 2019 , 100,	30
698	First-principles investigation of equilibrium K isotope fractionation among K-bearing minerals. 2019 , 264, 30-42	22
697	The Chemical Bond between Transition Metals and Oxygen: Electronegativity, d-Orbital Effects, and Oxophilicity as Descriptors of Metal-Oxygen Interactions. 2019 , 123, 18432-18444	37
696	Unified Assessment of the Effects of Van der Waals Interactions on the Structural and Electronic Properties of Some Layered Organic Solids [(BEDT-TTF) ₂ X]. 2019 , 9, 348	

695	DFT+U in Dudarev's formulation with corrected interactions between the electrons with opposite spins: The form of Hamiltonian, calculation of forces, and bandgap adjustments. 2019 , 151, 024102	7
694	Ab initio study of electronic structure properties of CaAF ₄ As ₄ (A = K, Rb and Cs) superconductors. 2019 , 169, 109114	1
693	Interrogation of fractional crystallization behavior of a newly exploited chiral resolution method for racemic 1-(pyridin-2-yl)ethylamine via DFT-D3 calculations of cohesive energy. 2019 , 6, 2325-2338	0
692	Determining the anisotropy and exchange parameters of polycrystalline spin-1 magnets. 2019 , 21, 093025	4
691	A first principles study on the ground state properties of three ferromagnetic skutterudites NdB ₄ As ₁₂ (B = Fe, Ru, Os). 2019 , 6, 106124	3
690	Machine Learning Interatomic Potentials as Emerging Tools for Materials Science. 2019 , 31, e1902765	177
689	Statistical learning goes beyond the d-band model providing the thermochemistry of adsorbates on transition metals. 2019 , 10, 4687	42
688	De novo exploration and self-guided learning of potential-energy surfaces. 2019 , 5,	73
687	Highly accurate local basis sets for large-scale DFT calculations in conquest. 2019 , 58, 100503	10
686	Data-Driven Materials Science: Status, Challenges, and Perspectives. 2019 , 6, 1900808	162
685	Unexpected magnetic behavior of Ga doped CuFe _{1-x} Ga _x O ₂ delafossite, x = 0.04: First principle calculation and Monte Carlo simulation. 2019 , 134, 1	4
684	A review on computational modelling of individual device components and interfaces of perovskite solar cells using DFT. 2019 ,	1
683	A High-Throughput Computational Study Driven by the AiiDA Materials Informatics Framework and the PAULING FILE as Reference Database. 2019 , 149-170	1
682	Ab Initio Calculation of Equilibrium Isotopic Fractionations of Potassium and Rubidium in Minerals and Water. 2019 , 3, 2601-2612	29
681	Ground-State and Thermodynamical Properties of Uranium Mononitride from Anharmonic First-Principles Theory. 2019 , 9, 3914	9
680	Relative Abundance of [Formula: see text] Topological Order in Exfoliable Two-Dimensional Insulators. 2019 , 19, 8431-8440	27
679	Ligand-Modified Boron-Doped Diamond Surface: DFT Insights into the Electronic Properties of Biofunctionalization. 2019 , 12,	2
678	A study of properties of palladium metal as a component of fuel cells. 2019 , 6, 105540	3

677	Graphite N-C-P dominated three-dimensional nitrogen and phosphorus co-doped holey graphene foams as high-efficiency electrocatalysts for Zn-air batteries. 2019 , 11, 17010-17017	29
676	IRMOF-74()-Mg: a novel catalyst series for hydrogen activation and hydrogenolysis of C-O bonds. 2019 , 10, 9880-9892	17
675	A review of atomistic simulation methods for surface physical-chemistry phenomena applied to froth flotation. 2019 , 143, 106020	37
674	Studies of electronic structure across a quantum phase transition in CeRhSb _{1-x} Sn _x . 2019 , 92, 1	1
673	Aspartic acid adsorption on thermoelectric surfaces. 2019 , 496, 143716	
672	Assessment of Approximate Methods for Anharmonic Free Energies. 2019 , 15, 5845-5857	19
671	Design and Synthesis of Ir/Ru Pyrochlore Catalysts for the Oxygen Evolution Reaction Based on Their Bulk Thermodynamic Properties. 2019 , 11, 37748-37760	36
670	Hierarchy of Commonly Used DFT Methods for Predicting the Thermochemistry of Rh-Mediated Chemical Transformations. 2019 , 4, 15435-15443	7
669	Incommensurate grain boundary in silicon and the silver-ratio sequence. 2019 , 100,	
668	Experimental and Theoretical Study of Surface-Enhanced Raman Spectra of Sulfadiazine Adsorbed on Nanoscale Gold Colloids. 2019 , 123, 9199-9208	5
667	Laser-Beam-Patterned Topological Insulating States on Thin Semiconducting MoS ₂ . 2019 , 123, 146803	13
666	Synthesis of magnesium-nitrogen salts of polynitrogen anions. 2019 , 10, 4515	39
665	Formation of hBN monolayers through nitridation of epitaxial silicene on diboride thin films. 2019 , 126, 135305	2
664	Reproducibility and the Concept of Numerical Solution. 2019 , 29, 19-36	4
663	Redox-active metal-organic frameworks for energy conversion and storage. 2019 , 7, 16571-16597	127
662	In Situ X-ray Photoelectron Spectroscopy Detects Multiple Active Sites Involved in the Selective Anaerobic Oxidation of Methane in Copper-Exchanged Zeolites. 2019 , 9, 6728-6737	19
661	Database of novel magnetic materials for high-performance permanent magnet development. 2019 , 168, 188-202	21
660	A review on non-relativistic, fully numerical electronic structure calculations on atoms and diatomic molecules. 2019 , 119, e25968	12

659	The Compendium: A Practical Guide to Theoretical Photoemission Spectroscopy. 2019 , 7, 377	139
658	Influence of strain and substitution on magnetocrystalline anisotropy of R ₂ Fe ₁₄ B (R=Pr, Dy and Y). 2019 , 488, 165370	
657	Theory and practice of modeling van der Waals interactions in electronic-structure calculations. 2019 , 48, 4118-4154	70
656	2DMatPedia, an open computational database of two-dimensional materials from top-down and bottom-up approaches. 2019 , 6, 86	92
655	Local Lattice Distortion Mediated Formation of Stacking Faults in Mg Alloys. 2019 ,	
654	Emerging inorganic solar cell efficiency tables (Version 1). 2019 , 1, 032001	39
653	Combining Pseudopotential and All Electron Density Functional Theory for the Efficient Calculation of Core Spectra Using a Multiresolution Approach. 2019 , 123, 4465-4474	5
652	Metallization and positive pressure dependency of bandgap in solid neon. 2019 , 150, 111103	5
651	Superstrong Noncovalent Interface between Melamine and Graphene Oxide. 2019 , 11, 17068-17078	12
650	Huge power factor in p-type half-Heusler alloys NbFeSb and TaFeSb. 2019 , 2, 035002	18
649	Ab initio calculation of multilayer magnetic structures by VASP on OpenPOWER high performance system. 2019 , 1163, 012059	
648	Towards Oxide Electronics: a Roadmap. 2019 , 482, 1-93	160
647	Adsorption of formaldehyde on transition metal doped monolayer MoS ₂ : A DFT study. 2019 , 484, 1244-1252	38
646	An Atomistic Understanding of the Unusual Thermal Behavior of the Molecular Oxide TcO. 2019 , 58, 5468-5475	1
645	Ultrathin Amorphous Titania on Nanowires: Optimization of Conformal Growth and Elucidation of Atomic-Scale Motifs. 2019 , 19, 3457-3463	6
644	Network analysis of synthesizable materials discovery. 2019 , 10, 2018	40
643	Static subspace approximation for the evaluation of G ₀ W ₀ quasiparticle energies within a sum-over-bands approach. 2019 , 99,	2
642	Fine-grained Material Associated with a Large Sulfide returned from Comet 81P/Wild 2. 2019 , 54, 1069-1091	2

641	The influence of hydroxy groups on the adsorption of three-carbon alcohols on Ni(111), Pd(111) and Pt(111) surfaces: a density functional theory study within the D3 dispersion correction. 2019 , 21, 8434-8444	12
640	Applications of DFT + DMFT in Materials Science. 2019 , 49, 31-52	18
639	Electronic properties of heterogenized Ru(II) polypyridyl photoredox complexes on covalent triazine frameworks. 2019 , 7, 8433-8442	4
638	DFT Computed Dielectric Response and THz Spectra of Organic Co-Crystals and Their Constituent Components. 2019 , 24,	2
637	New frontiers for the materials genome initiative. 2019 , 5,	171
636	Density-functional theory for plutonium. 2019 , 68, 1-47	27
635	Main-group test set for materials science and engineering with user-friendly graphical tools for error analysis: systematic benchmark of the numerical and intrinsic errors in state-of-the-art electronic-structure approximations. 2019 , 21, 013025	10
634	The evolving landscape for alloy design. 2019 , 44, 238-246	14
633	Optical, charge transport and magnetic properties of palladium retrieved from photometric measurements: approaching the quantum mechanics background. 2019 , 94, 055101	1
632	Structure prediction drives materials discovery. 2019 , 4, 331-348	242
631	Rare-earth magnetic nitride perovskites. 2019 , 2, 025003	14
630	Advances in Density-Functional Calculations for Materials Modeling. 2019 , 49, 1-30	56
629	Hyperspatial optimization of structures. 2019 , 99,	9
628	Convergence and machine learning predictions of Monkhorst-Pack k-points and plane-wave cut-off in high-throughput DFT calculations. 2019 , 161, 300-300	24
627	Role of defects in determining the magnetic ground state of ytterbium titanate. 2019 , 10, 637	19
626	First-principles-based prediction of yield strength in the RhIrPdPtNiCu high-entropy alloy. 2019 , 5,	47
625	Accurate molecular polarizabilities with coupled cluster theory and machine learning. 2019 , 116, 3401-3406	71
624	Strong interband interaction in the excitonic insulator phase of Ta ₂ NiSe ₅ . 2019 , 99,	24

623	From DFT to machine learning: recent approaches to materials science – review. 2019 , 2, 032001	206
622	Electronic band structure and proximity to magnetic ordering in the chiral cubic compound CrGe. 2019 , 99,	3
621	Electronic structure of CeCo ₁₁ Be Ge ₃ studied by X-ray photoelectron spectroscopy and first-principles calculations. 2019 , 787, 744-750	2
620	Crystal field coefficients for yttrium analogues of rare-earth/transition-metal magnets using density-functional theory in the projector-augmented wave formalism. 2019 , 31, 305901	7
619	STEM materials: a new frontier for an intelligent sustainable world. 2019 , 1,	1
618	Challenges for Verifying and Validating Scientific Software in Computational Materials Science. 2019 ,	1
617	Synthesis, characterization and modeling of self-assembled porphyrin nanorods. 2019 , 23, 1346-1354	2
616	Photorealistic modelling of metals from first principles. 2019 , 5,	10
615	Charge-induced electromechanical actuation of two-dimensional hexagonal and pentagonal materials. 2019 , 21, 22377-22384	9
614	Predicted high thermoelectric performance in a two-dimensional indium telluride monolayer and its dependence on strain. 2019 , 21, 24695-24701	15
613	A first-principles study of magnetic properties of Zn _{0.94} Mg _{0.01} Mn _{0.05} O. 2019 , 6, 126118	3
612	Assessing Relativistic Effects and Electron Correlation in the Actinide Metals Th to Pu. 2019 , 9, 5020	13
611	Equation of state of hexagonal-close-packed rhenium in the terapascal regime. 2019 , 100,	5
610	Biological Material Interfaces as Inspiration for Mechanical and Optical Material Designs. 2019 , 119, 12279-12336	6
609	Photo-accelerated fast charging of lithium-ion batteries. 2019 , 10, 4946	32
608	Strategies to break linear scaling relationships. 2019 , 2, 971-976	127
607	A DFT study of energetic and structural properties of a full turn of A-form DNA under relaxed and stretching conditions. 2019 , 151, 215102	5
606	MOLC. A reversible coarse grained approach using anisotropic beads for the modelling of organic functional materials. 2019 , 21, 26195-26211	11

605	Correlated materials design: prospects and challenges. 2019 , 82, 012504	21
604	An In Situ Surface-Enhanced Infrared Absorption Spectroscopy Study of Electrochemical CO ₂ Reduction: Selectivity Dependence on Surface C-Bound and O-Bound Reaction Intermediates. 2019 , 123, 5951-5963	78
603	Theoretical insights into photo-induced electron transfer at BiOX (X = F, Cl, Br, I) (001) surfaces and interfaces. 2019 , 21, 868-875	34
602	Professor Jan Vĕř and His Contributions Towards the Implementing of Ab Initio Data into the CALPHAD Method and Extension of the Phase Diagram Calculations Down to 0 K. 2019 , 40, 3-9	
601	Push it to the limit: comparing periodic and local approaches to density functional theory for intermolecular interactions. 2019 , 117, 1298-1305	3
600	DFT calculations of energy dependent XPS valence band spectra. 2019 , 230, 1-9	8
599	CO ₂ reduction by H ₂ to CHO on Ru(0001): DFT evaluation of three pathways. 2019 , 681, 54-58	8
598	Calculation of Magnetic Exchange Interactions and Construction of a Spin Model for Low-Dimensional Magnetic Compounds. 2019 , 48, 1480-1485	
597	Effects of electron beam generated lattice defects on the periodic lattice distortion structure in 1T-TaS ₂ and 1T-TaSe ₂ thin layers. 2019 , 99,	3
596	Understanding non-covalent interactions in larger molecular complexes from first principles. 2019 , 150, 010901	29
595	Revealing Photoluminescence Modulation from Layered Halide Perovskite Microcrystals upon Cyclic Compression. 2019 , 31, e1805608	12
594	Stability of room temperature compensated half-metallicity in Cr-based Inverse-Heusler Compounds. 2019 , 19, 193-197	10
593	Tuning the Magnetic Properties of FeCo Thin Films through the Magnetoelastic Effect Induced by the Au Underlayer Thickness. 2019 , 11, 1529-1537	10
592	An NMR crystallography investigation of furosemide. 2019 , 57, 191-199	4
591	Formation and migration of point defects in tungsten carbide: Unveiling the sluggish bulk self-diffusivity of WC. 2019 , 39, 165-172	14
590	A first-principles reassessment of the Fe-N phase diagram in the low-nitrogen limit. 2019 , 775, 758-768	8
589	SternheimerGW: A program for calculating GW quasiparticle band structures and spectral functions without unoccupied states. 2020 , 247, 106856	7
588	Projector augmented-wave pseudopotentials for uranium-based compounds. 2020 , 171, 109237	8

587	Superconducting Hydrides Under Pressure. 2020 , 11, 57-76	70
586	Metric based on the arctangents of the logderivatives for evaluating scattering properties of pseudopotentials. 2020 , 247, 106929	0
585	Towards photoferroic materials by design: recent progress and perspectives. 2020 , 2, 011001	7
584	Structural and magnetic investigations on Cu-doped MnV ₂ O ₆ compound: Experiment and theory. 2020 , 497, 165995	0
583	Ab-initio approach to the stability and the structural, electronic and magnetic properties of the (001) ZnFe ₂ O ₄ surface terminations. 2020 , 499, 143859	8
582	Recent Progress in Lithium Niobate: Optical Damage, Defect Simulation, and On-Chip Devices. 2020 , 32, e1806452	68
581	Surface and electronic properties of rutile TiO ₂ thin films coated with PbO ₂ . 2020 , 171, 109222	7
580	The GIPAW approach for the study of local structures and the electric field gradients at Cd and Ta impurity sites. Application to doped yttria ceramics. 2020 , 171, 109224	3
579	Equilibrium inter-mineral titanium isotope fractionation: Implication for high-temperature titanium isotope geochemistry. 2020 , 269, 540-553	18
578	QuantumATK: an integrated platform of electronic and atomic-scale modelling tools. 2020 , 32, 015901	330
577	A theoretical study of gas adsorption on calcite for CO ₂ enhanced natural gas recovery. 2020 , 504, 144575	11
576	Nickel isotope fractionation during metal-silicate differentiation of planetesimals: Experimental petrology and ab initio calculations. 2020 , 269, 238-256	6
575	Adsorption of different PAM structural units on kaolinite (0 0 1) surface: Density functional theory study. 2020 , 504, 144324	20
574	Variational projector augmented-wave method: theoretical analysis and preliminary numerical results. 2020 , 144, 271-321	2
573	Vibrational Response of Felodipine in the THz Domain: Optical and Neutron Spectroscopy Versus Plane-Wave DFT Modeling. 2020 , 41, 1301-1336	5
572	Exploring the Reliability of DFT Calculations of the Infrared and Terahertz Spectra of Sodium Peroxodisulfate. 2020 , 41, 382-413	3
571	Li-decorated carbyne for hydrogen storage: charge induced polarization and van't Hoff hydrogen desorption temperature. 2020 , 4, 691-699	8
570	Comparison of computational methods for the electrochemical stability window of solid-state electrolyte materials. 2020 , 8, 1347-1359	27

569	Questaal: A package of electronic structure methods based on the linear muffin-tin orbital technique. 2020 , 249, 107065	39
568	High-pressure, high-temperature phase stability of iron-poor dolomite and the structures of dolomite-IIIc and dolomite-V. 2020 , 299, 106403	12
567	The Abinitproject: Impact, environment and recent developments. 2020 , 248, 107042	143
566	Accuracy of Dispersion-Corrected Density Functional Theory Calculations of Elastic Tensors of Organic Molecular Structures. 2020 , 20, 206-213	6
565	Intertwined magnetic sublattices in the double perovskite compound LaSrNiReO6. 2020 , 102,	1
564	Measuring the Intra-Atomic Exchange Energy in Rare-Earth Adatoms. 2020 , 10,	3
563	Density Functional Theory and Thermodynamics Modeling of Inner-Sphere Oxyanion Adsorption on the Hydroxylated AlO(001) Surface. 2020 , 36, 13166-13180	6
562	Role of higher-order exchange interactions for skyrmion stability. 2020 , 11, 4756	18
561	Reproducibility of potential energy surfaces of organic/metal interfaces on the example of PTCDA on Ag(111). 2020 , 153, 104701	7
560	Pressure-Induced Polymerization of Polycyclic Arene-Perfluoroarene Cocrystals: Single Crystal X-ray Diffraction Studies, Reaction Kinetics, and Design of Columnar Hydrofluorocarbons. 2020 , 142, 18907-18923	19
559	Novel sulfur hydrides synthesized at extreme conditions. 2020 , 102,	16
558	Room-temperature superconductivity in a carbonaceous sulfur hydride. 2020 , 586, 373-377	251
557	Highly Robust Oxynitride Phosphor against Thermal Oxidization and Hydrolysis. 2020 , 8, 12286-12294	11
556	Cost-effective composite methods for large-scale solid-state calculations. 2020 , 224, 292-308	3
555	Influence of high-energy local orbitals and electron-phonon interactions on the band gaps and optical absorption spectra of hexagonal boron nitride. 2020 , 102,	7
554	Tuning Hydrogen Storage Properties of Carbon Nanosheets through Selected Foreign Metal Functionalization. 2020 , 124, 16827-16837	5
553	Density Functional Theories and Coordination Chemistry. 2020 ,	2
552	On the Possibility of Helium Adsorption in Nitrogen Doped Graphitic Materials. 2020 , 10, 5832	5

551	Generalizing Double-Hybrid Density Functionals: Impact of Higher-Order Perturbation Terms. 2020 , 16, 7413-7430	7
550	Trends in the Activation of Light Alkanes on Transition-Metal Surfaces. 2020 , 124, 27503-27510	3
549	Pressure-Induced Phase Transitions in Danburite-Type Borosilicates. 2020 , 124, 26048-26061	2
548	Fe-doped Na _{0.47} Bi _{0.47} Ba _{0.06} Ti _{0.98-x} V _{0.02} Fe _x O ₃ : Structure correlated vibrational, optical and electrical properties. 2020 , 848, 156503	4
547	Neural network potential from bispectrum components: A case study on crystalline silicon. 2020 , 153, 054118	5
546	error estimation for the non-self-consistent Kohn-Sham equations. 2020 , 224, 227-246	3
545	Activity origin and design principles for atomic vanadium anchoring on phosphorene monolayer for nitrogen reduction reaction. 2020 , 13, 2925-2932	18
544	Efficient Kr/Xe separation from triangular g-C ₃ N ₄ nanopores, a simulation study. 2020 , 8, 17747-17755	3
543	Ab initio study of the half-metallic full-Heusler compounds Co ₂ ZAl [Z = Sc, Ti, V, Cr, Mn, Fe]; the role of electronic correlations. 2020 , 25, 101498	4
542	An artificial intelligence-aided virtual screening recipe for two-dimensional materials discovery. 2020 , 6,	14
541	Morphology and strain control of hierarchical cobalt oxide nanowire electrocatalysts via solvent effect. 2020 , 13, 3130-3136	7
540	On the planarity of the cyclobutane ring in the crystal of dimethyl 2,4-bis(3,4-dimethoxyphenyl)cyclobutane-1,3-dicarboxylate: a natural bond orbital and Hirshfeld surface analysis study. 2020 , 44, 15515-15525	2
539	Relativistic correction scheme for core-level binding energies from GW. 2020 , 153, 114110	10
538	First-principles study of topologically protected vortices and ferroelectric domain walls in hexagonal YGaO ₃ . 2020 , 102,	5
537	Effects of pH and ions on the morphological evolution of boehmite prepared by hydrothermal treatment of ultrafine Bayer gibbsite. 2020 , 22, 6983-6992	5
536	First-Principles Investigation of Single-Atom Ni ₁ -C ₃ N ₄ as an Efficient Catalyst for Direct Reduction of NO with CO. 2020 , 34, 12792-12799	4
535	Organic-to-inorganic structural chirality transfer in a 2D hybrid perovskite and impact on Rashba-Dresselhaus spin-orbit coupling. 2020 , 11, 4699	65
534	Preface. 2020 , xix-xxiii	

533 Introduction. **2020**, 1-14

532 Overview. **2020**, 15-59

531 Theoretical Background. **2020**, 60-80

530 Periodic Solids and Electron Bands. **2020**, 81-108

529 Uniform Electron Gas and sp-Bonded Metals. **2020**, 109-128

528 Density Functional Theory: Foundations. **2020**, 129-144

527 The Kohn-Sham Auxiliary System. **2020**, 145-170

526 Functionals for Exchange and Correlation I. **2020**, 171-187

525 Functionals for Exchange and Correlation II. **2020**, 188-214

524 Electronic Structure of Atoms. **2020**, 215-229

523 Pseudopotentials. **2020**, 230-258

522 Overview of Chapters 12-18. **2020**, 259-261

521 Plane Waves and Grids: Basics. **2020**, 262-282

520 Plane Waves and Real-Space Methods: Full Calculations. **2020**, 283-294

519 Localized Orbitals: Tight-Binding. **2020**, 295-319

518 Localized Orbitals: Full Calculations. **2020**, 320-331

517 Augmented Functions: APW, KKR, MTO. **2020**, 332-364

516 Augmented Functions: Linear Methods. **2020**, 365-385

515 Locality and Linear-Scaling $O(N)$ Methods. **2020**, 386-410

514 Quantum Molecular Dynamics (QMD). **2020**, 411-426

513 Response Functions: Phonons and Magnons. **2020**, 427-445

512 Excitation Spectra and Optical Properties. **2020**, 446-464

511 Surfaces, Interfaces, and Lower-Dimensional Systems. **2020**, 465-480

510 Wannier Functions. **2020**, 481-498

509 Polarization, Localization, and Berry Phases. **2020**, 499-516

508 Topology of the Electronic Structure of a Crystal: Introduction. **2020**, 517-530

507 Two-Band Models: Berry Phase, Winding, and Topology. **2020**, 531-546

506 Topological Insulators I: Two Dimensions. **2020**, 547-568

505 Topological Insulators II: Three Dimensions. **2020**, 569-580

504 Functional Equations. **2020**, 581-583

503 LSDA and GGA Functionals. **2020**, 584-586

502 Adiabatic Approximation. **2020**, 587-589

501 Perturbation Theory, Response Functions, and Green's Functions. **2020**, 590-599

500 Dielectric Functions and Optical Properties. **2020**, 600-606

499 Coulomb Interactions in Extended Systems. **2020**, 607-619

498 Stress from Electronic Structure. **2020**, 620-626

497 Energy and Stress Densities. **2020**, 627-636

496 Alternative Force Expressions. **2020**, 637-643

495 Scattering and Phase Shifts. **2020**, 644-646

494 Useful Relations and Formulas. **2020**, 647-650

493 Numerical Methods. **2020**, 651-660

492 Iterative Methods in Electronic Structure. **2020**, 661-676

491 Two-Center Matrix Elements: Expressions for Arbitrary Angular Momentum l. **2020**, 677-685

490 Dirac Equation and Spin-Orbit Interaction. **2020**, 686-696

489 Berry Phase, Curvature, and Chern Numbers. **2020**, 697-700

488 Quantum Hall Effect and Edge Conductivity. **2020**, 701-703

487 Index. **2020**, 756-762

486 Density functional theory and 3D-RISM-KH molecular theory of solvation studies of CO reduction on Cu-, CuO-, Fe-, and FeO-based nanocatalysts. **2020**, 26, 267 4

485 Small data materials design with machine learning: When the average model knows best. **2020**, 128, 054901 9

484 Identifying materials with charge-spin physics using charge-spin susceptibility computed from first principles. **2020**, 153, 074105 2

483 The Tetragonal Monoxide of Platinum: A New Platform for Investigating Nodal-Line and Nodal-Point Semimetallic Behavior. **2020**, 8, 704 5

482 Nonparametric Local Pseudopotentials with Machine Learning: A Tin Pseudopotential Built Using Gaussian Process Regression. **2020**, 124, 11111-11124 4

481 Influence of Pr substitution on the physical properties of the $Ce_{1-x}Pr_xCoGe_3$ system: Combined experimental and first-principles study. **2020**, 102, 2

480 First-principles study on the stability and electronic structure of monolayer GaSe with trigonal-antiprismatic structure. **2020**, 102, 4

479	Lithium Niobate Single Crystals and Powders ReviewedPart II. 2020 , 10, 990	7
478	Single-Molecule Detection of Acetylcholine by Translating the Neuronal Signal to a Single Distinct Electronic Peak.. 2020 , 3, 6888-6896	3
477	MXenes: New Horizons in Catalysis. 2020 , 10, 13487-13503	87
476	Electrocatalytic reduction of CO ₂ to ethylene and ethanol through hydrogen-assisted C ₁ coupling over fluorine-modified copper. 2020 , 3, 478-487	286
475	Yield strength and misfit volumes of NiCoCr and implications for short-range-order. 2020 , 11, 2507	61
474	Diffusion Properties of Oxygen in the TiAl Alloy. 2020 , 130, 579-590	8
473	Validation of Pseudopotential Calculations for the Electronic Band Gap of Solids. 2020 , 16, 3620-3627	9
472	First-principles study of elastic and thermal properties of scheelite-type molybdates and tungstates. 2020 , 24, 101089	5
471	CP2K: An electronic structure and molecular dynamics software package - Quickstep: Efficient and accurate electronic structure calculations. 2020 , 152, 194103	421
470	Fermi surface of LaFeP-a detailed density functional study. 2020 , 32, 025503	0
469	A Semiempirical Method to Detect and Correct DFT-Based Gas-Phase Errors and Its Application in Electrocatalysis. 2020 , 10, 6900-6907	36
468	Flexibilities of wavelets as a computational basis set for large-scale electronic structure calculations. 2020 , 152, 194110	21
467	High-Pressure Polymeric Nitrogen Allotrope with the Black Phosphorus Structure. 2020 , 124, 216001	49
466	Exploring chemical compound space with quantum-based machine learning. 2020 , 4, 347-358	87
465	Structural investigation of ternary PdRuM (M = Pt, Rh, or Ir) nanoparticles using first-principles calculations.. 2020 , 10, 16527-16536	0
464	Application of the training of density functional theory potentials within machine learning to adsorptions and reaction paths on Platinum surfaces. 2020 , 253, 123407	1
463	Analysis of Electronic and Optical Properties of Pristine LiNbO ₃ Using First-Principle Calculations. 2020 ,	
462	Why are MoS ₂ monolayers not a good catalyst for the oxygen evolution reaction?. 2020 , 528, 146591	10

461	(Sm,Zr)Fe ₁₂ Mx (M=Zr,Ti,Co) for Permanent-Magnet Applications: Ab Initio Material Design Integrated with Experimental Characterization. 2020 , 13,	16
460	Fermi surface investigation of the noncentrosymmetric superconductor PdBi . 2020 , 101,	1
459	Phase Stability in U-6Nb Alloy Doped with Ti from the First Principles Theory. 2020 , 10, 3417	4
458	Predicting HSE band gaps from PBE charge densities via neural network functionals. 2020 , 32, 155901	8
457	Roadmap on multiscale materials modeling. 2020 , 28, 043001	40
456	NMR crystallography of molecular organics. 2020 , 118-119, 10-53	49
455	ABINIT: Overview and focus on selected capabilities. 2020 , 152, 124102	52
454	Octopus, a computational framework for exploring light-driven phenomena and quantum dynamics in extended and finite systems. 2020 , 152, 124119	86
453	Time-dependent density-functional theory for periodic solids: assessment of excitonic exchange-correlation kernels. 2020 , 2, 023002	12
452	Accuracy of Localized Resolution of the Identity in Periodic Hybrid Functional Calculations with Numerical Atomic Orbitals. 2020 , 11, 3082-3088	6
451	Structural and transport properties of Cu/Ta(N)/Cu interfaces in vertical interconnects. 2020 , 127, 125705	2
450	Accurate Ab Initio Calculations on Various PV-Based Materials: Which Functional to Be Used?. 2020 , 124, 8467-8478	7
449	Thermodynamics of Uranium Tri-Iodide from Density-Functional Theory. 2020 , 10, 3914	2
448	On the use of DFT+U to describe the electronic structure of TiO nanoparticles: (TiO) as a case study. 2020 , 152, 244107	2
447	High thermal conductance across c-BN/diamond interface. 2020 , 108, 107979	5
446	Role of a higher-dimensional interaction in stabilizing charge density waves in quasi-one-dimensional NbSe ₃ revealed by angle-resolved photoemission spectroscopy. 2020 , 101,	4
445	Nanoscale Scanning Electrochemical Cell Microscopy and Correlative Surface Structural Analysis to Map Anodic and Cathodic Reactions on Polycrystalline Zn in Acid Media. 2020 , 167, 041507	18
444	A perspective on conventional high-temperature superconductors at high pressure: Methods and materials. 2020 , 856, 1-78	132

443	WIEN2k: An APW+lo program for calculating the properties of solids. 2020 , 152, 074101	408
442	Machine learning: Accelerating materials development for energy storage and conversion. 2020 , 2, 553-576	86
441	Single crystal neutron and magnetic measurements of RbMn(VO)CO and KCo(VO)CO with mixed honeycomb and triangular magnetic lattices. 2020 , 49, 4323-4335	5
440	Direct Comparison of Many-Body Methods for Realistic Electronic Hamiltonians. 2020 , 10,	46
439	Towards an ab initio theory for the temperature dependence of electric field gradients in solids: Application to hexagonal lattices of Zn and Cd. 2020 , 101,	1
438	The Exploration of Chemical Reaction Networks. 2020 , 71, 121-142	46
437	First Principles Investigation of Cold Curves of Metals. 2020 , 60, 897-904	0
436	DFT-based study of the bulk tin mixed-halide CsSn ₁₋₃ xBr _x perovskite. 2020 , 178, 109619	8
435	Pressure-induced antiferromagnetic dome in the heavy-fermion Yb ₂ Pd ₂ In _{1-x} Sn _x system. 2020 , 101,	1
434	Tuning metal oxide defect chemistry by thermochemical quenching. 2020 , 22, 6308-6317	2
433	Quasi-degenerate states and their dynamics in oxygen deficient reducible metal oxides. 2020 , 152, 050901	12
432	Dirac's equation and its implications for density functional theory based calculations of materials containing heavy elements. 2020 , 101,	4
431	Metal-free two-dimensional phosphorus carbide as an efficient electrocatalyst for hydrogen evolution reaction comparable to platinum. 2020 , 71, 104603	22
430	Performance and Cost Assessment of Machine Learning Interatomic Potentials. 2020 , 124, 731-745	185
429	Clear Rules the Electronic Properties of 2D π -Conjugated Frameworks: Mind the Gap. 2020 , 26, 6569-6575	3
428	Enhancing the partial oxidation of gasoline with Mo-doped Ni catalysts for SOFC applications: An integrated experimental and DFT study. 2020 , 266, 118626	10
427	Structural Tolerance Factor Approach to Defect-Resistant I ² -II-IV-X ₄ Semiconductor Design. 2020 , 32, 1636-1649	14
426	FCHL revisited: Faster and more accurate quantum machine learning. 2020 , 152, 044107	108

425	Periodic F-defects on the MgO surface as potential single-defect catalysts with non-linear optical properties. 2020 , 532, 110680	13
424	On-Surface Synthesis of Cumulene-Containing Polymers via Two-Step Dehalogenative Homocoupling of Dibromomethylene-Functionalized Tribenzoazulene. 2020 , 132, 13383-13389	8
423	Classical and Emerging Characterization Techniques for Investigation of Ion Transport Mechanisms in Crystalline Fast Ionic Conductors. 2020 , 120, 5954-6008	66
422	On-Surface Synthesis of Cumulene-Containing Polymers via Two-Step Dehalogenative Homocoupling of Dibromomethylene-Functionalized Tribenzoazulene. 2020 , 59, 13281-13287	11
421	Geometric landscapes for material discovery within energy-structure-function maps. 2020 , 11, 5423-5433	12
420	Identification of hydrogen bonds using quantum electrodynamics. 2020 , 120, e26237	0
419	Uncertainty quantification in materials modeling. 2020 , 1-40	4
418	Atomically scale design of van der Waals heterostructures as photocatalysts. 2020 , 511-525	0
417	The uncertainty pyramid for electronic-structure methods. 2020 , 41-76	3
416	Data-driven acceleration of first-principles saddle point and local minimum search based on scalable Gaussian processes. 2020 , 119-168	
415	Multiscale modeling approaches for waste biorefinery. 2020 , 425-453	
414	Towards band gap engineering via biaxial and axial strain in group IV crystals. 2020 , 181, 109729	1
413	GPU acceleration of all-electron electronic structure theory using localized numeric atom-centered basis functions. 2020 , 254, 107314	14
412	Rational ligand choice extends the SABRE substrate scope. 2020 , 56, 9336-9339	15
411	Advances in the synthesis and structure of Ekanaphite: a multitool and multiscale study. 2020 , 22, 3130-3143	5
410	Synthesis of metal-free lightweight materials with sequence-encoded properties. 2020 , 8, 8752-8760	5
409	Improved description of perovskite oxide crystal structure and electronic properties using self-consistent Hubbard U corrections from ACBN0. 2020 , 101,	5
408	Electronic, optical and elastic properties of cubic zirconia (c-ZrO ₂) under pressure: A DFT study. 2021 , 604, 412462	4

407	Turning chemistry into information for heterogeneous catalysis. 2021 , 121, e26382	7
406	Electronic structure of LiOsO ₃ : Electron energy-loss spectroscopy and first-principles study. 2021 , 323, 114099	3
405	An automated cluster surface scanning method for exploring reaction paths on metal-cluster surfaces. 2021 , 186, 110010	2
404	Workflows in AiiDA: Engineering a high-throughput, event-based engine for robust and modular computational workflows. 2021 , 187, 110086	18
403	Interfacial microstructures and adsorption mechanisms of benzohydroxamic acid on Pb ²⁺ -activated cassiterite (1 1 0) surface. 2021 , 541, 148506	4
402	Surface and interface engineering of two-dimensional bismuth-based photocatalysts for ambient molecule activation. 2021 , 9, 196-233	19
401	Effect of pseudopotential choice on the calculated electron and phonon band structures of palladium hydride and its vacancy defect phases. 2021 , 46, 943-954	2
400	Uncertainty Quantification in Atomistic Modeling of Metals and Its Effect on Mesoscale and Continuum Modeling: A Review. 2021 , 73, 149	3
399	Integrating data mining and machine learning to discover high-strength ductile titanium alloys. 2021 , 202, 211-221	25
398	Computational Study of Transition-Metal Substitutions in Rutile TiO ₂ (110) for Photoelectrocatalytic Ammonia Synthesis. 2021 , 151, 1142-1154	2
397	A structure map for AB ₂ type 2D materials using high-throughput DFT calculations. 2021 , 2, 4392-4413	4
396	Identification of synthesisable crystalline phases of water as a prototype for the challenges of computational materials design. 2021 , 23, 252-263	
395	Magnetocrystalline anisotropy of Fe ₁₆ N ₂ under various DFT approaches. 2021 , 11, 015039	3
394	Enhanced optical absorption of rutile TiO ₂ through (Sm, C) codoping: a first-principles study. 2021 , 53, 1	3
393	Defect-nucleated phase transition in atomically-thin WS ₂ . 2021 , 8, 025017	4
392	Exploring the nature of the fergusonite↔scheelite phase transition and ionic conductivity enhancement by Mo ⁶⁺ doping in LaNbO ₄ . 2021 , 9, 4091-4102	5
391	All-electron periodic G ₀ W ₀ implementation with numerical atomic orbital basis functions: Algorithm and benchmarks. 2021 , 5,	11
390	Towards fully automated GW band structure calculations: What we can learn from 60.000 self-energy evaluations. 2021 , 7,	3

389	Modulation of the electronic states and magnetic properties of nickel catecholdithiolene complex by oxidation-coupled deprotonation. 2021 , 9, 10718-10726	1
388	Na ₂ La ₂ B ₁₀ O ₁₉ : a new lanthanum sodium borate with infinite 2D layer 2[B ₁₀ O ₁₉] ₈ and moderate birefringence. 2021 , 45, 13592-13598	0
387	Mass Dependence of Equilibrium Oxygen Isotope Fractionation in Carbonate, Nitrate, Oxide, Perchlorate, Phosphate, Silicate, and Sulfate Minerals. 2021 , 86, 137-178	10
386	Hydrogenation of TiO ₂ nanosheets and nanoparticles: typical reduction stages and orientation-related anisotropic disorder.	2
385	First-principles calculations of hybrid inorganic-organic interfaces: from state-of-the-art to best practice. 2021 , 23, 8132-8180	11
384	Elucidating the Influence of Electric Fields toward CO ₂ Activation on YSZ (111). 2021 , 11, 271	3
383	Calculation and interpretation of classical turning surfaces in solids. 2021 , 7,	1
382	Nitro-sonium nitrate (NONO ⁺) structure solution using single-crystal X-ray diffraction in a diamond anvil cell. 2021 , 8, 208-214	3
381	Elastic stiffness coefficients of thiourea from thermal diffuse scattering. 2021 , 54, 287-294	1
380	Anisotropic superconductivity in the spin-vortex antiferromagnetic superconductor CaK(Fe _{0.95} Ni _{0.05}) ₄ As ₄ . 2021 , 103,	1
379	Millisecond lattice gasification for high-density CO ₂ - and O ₂ -sieving nanopores in single-layer graphene. 2021 , 7,	15
378	DFT-based calculations of the magnetic hyperfine interactions at Cd sites in RCd (R = rare earth) compounds with the FP-LAPW ELK code. 2021 , 11, 025010	0
377	First-principles calculation of electroacoustic properties of wurtzite (Al,Sc)N. 2021 , 103,	15
376	High Li-ion conductivity in tetragonal LGPO: A comparative first-principles study against known LISICON and LGPS phases. 2021 , 5,	2
375	Polarons in materials. 2021 , 6, 560-586	58
374	Thermal Boundary Resistance at Graphene-Pentacene Interface Explored by A Data-Intensive Approach. 2021 ,	2
373	Efficient implementation of atom-density representations. 2021 , 154, 114109	16
372	A data fusion approach to optimize compositional stability of halide perovskites. 2021 , 4, 1305-1322	27

371	Efficient electronic passivation scheme for computing low-symmetry compound semiconductor surfaces in density-functional theory slab calculations. 2021 , 5,	
370	Measuring Density Functional Parameters from Electron Diffraction Patterns. 2021 , 126, 176402	0
369	Improved predictions of thermomechanical properties of molecular crystals from energy and dispersion corrected DFT. 2021 , 154, 164105	3
368	Synthesis of calcium orthocarbonate, Ca ₂ CO ₄ -Pnma at p, T-conditions of Earth's transition zone and lower mantle. 2021 ,	9
367	Epistemic issues in computational reproducibility: software as the elephant in the room. 2021 , 11, 1	2
366	Oxygen Evolution on MoS ₂ Edges: Activation through Surface Oxidation. 2021 , 125, 10397-10405	3
365	An approach based on random sampling and density functional theory to identify highly stable structures of ABX ₃ compounds. 2021 , 192, 110304	1
364	Chalcogenide perovskites for photovoltaics: current status and prospects. 2021 , 3, 034010	9
363	Compound-tunable embedding potential method and its application to calcium niobate crystal CaNb ₂ O ₆ with point defects containing tantalum and uranium. 2021 , 103,	3
362	Voltage-controlled magnetic anisotropy in antiferromagnetic MgO-capped MnPt films. 2021 , 5,	1
361	Electronic-structure methods for materials design. 2021 , 20, 736-749	24
360	Induced magnetization in Cu atoms at the Fe-Co/Cu ₃ Au(001) interface: X-ray magnetic circular dichroism experiments and theoretical results. 2021 , 548, 149215	0
359	Dimensionality reduction of complex reaction networks in heterogeneous catalysis: From linear-scaling relationships to statistical learning techniques. 2021 , 11, e1540	2
358	Best practices in machine learning for chemistry. 2021 , 13, 505-508	61
357	Quantum surface-response of metals revealed by acoustic graphene plasmons. 2021 , 12, 3271	11
356	Accurate frozen core approximation for all-electron density-functional theory. 2021 , 154, 224107	
355	Interplay between invasive single atom Pt and native oxygen vacancy in rutile TiO ₂ (110) surface: A theoretical study. 1	1
354	Computational Chemistry: The Exciting Opportunities and the Boring Details.	0

353	Sensitivity of the Fermi surface to the treatment of exchange and correlation. 2021 , 103,	1
352	Quasi-four-component method with numeric atom-centered orbitals for relativistic density functional simulations of molecules and solids. 2021 , 103,	2
351	Iron, magnesium, and titanium isotopic fractionations between garnet, ilmenite, fayalite, biotite, and tourmaline: Results from NRIXS, ab initio, and study of mineral separates from the Moosilauke metapelite. 2021 , 302, 18-45	8
350	Pseudopotentials for Electronic Structure Theory. 2021 , 125, 15103-15111	1
349	Symmetry-enforced topological nodal planes at the Fermi surface of a chiral magnet. 2021 , 594, 374-379	6
348	Integration of theory and experiment in the modelling of heterogeneous electrocatalysis.	14
347	The eruption of carbon chains in the oxidation of 2D $Ti_{n+1}C_n$ ($n = 1, 2, 3$) MXenes. 2021 , 550, 149310	3
346	Inside the electronic structure of the $Sm_3Fe_5O_{12}$ garnet: A mixed ab initio and experimental study. 2021 , 104,	1
345	Accelerating finite-temperature Kohn-Sham density functional theory with deep neural networks. 2021 , 104,	4
344	All-electron full-potential implementation of real-time TDDFT in exciting. 2021 , 3, 037001	1
343	Combining Machine Learning and Computational Chemistry for Predictive Insights Into Chemical Systems. 2021 , 121, 9816-9872	53
342	Wurtzite $ScAlN$, $InAlN$, and $GaAlN$ crystals, a comparison of structural, elastic, dielectric, and piezoelectric properties. 2021 , 130, 045102	8
341	Robust model benchmarking and bias-imbalance in data-driven materials science: a case study on MODNet. 2021 , 33,	2
340	Out-of-Plane Transport of 1T-TaS/Graphene-Based van der Waals Heterostructures. 2021 , 15, 11898-11907	7
339	Physics-Inspired Structural Representations for Molecules and Materials. 2021 , 121, 9759-9815	50
338	5f states in UGa_2 probed by x-ray spectroscopies. 2021 , 104,	0
337	Structural, Optical, and Electronic Properties of Two Quaternary Chalcogenide Semiconductors: $AgSrSiS$ and $AgSrGeS$. 2021 , 60, 12206-12217	2
336	Is $Mg_{17}Al_{12}$ ductile or brittle? A theoretical insight. 2021 ,	2

- 335 Structural, Physical, and Thermodynamic Properties of Aragonitic $\text{Ca}_x\text{Sr}_{1-x}\text{CO}_3$ Solid Solutions. **2021**, 125, 17474-17481
- 334 Systematic Investigation of Error Distribution in Machine Learning Algorithms Applied to the Quantum-Chemistry QM9 Data Set Using the Bias and Variance Decomposition. **2021**, 61, 4210-4223 3
- 333 The influence of chemical impurities on the properties of heavy rare-earth metals (Tb, Dy, Ho): Experimental and theoretical approaches. **2021**, 18, 101166 0
- 332 Gas Transport across Carbon Nitride Nanopores: A Comparison of van der Waals Functionals against the Random-Phase Approximation. **2021**, 125, 18896-18904 0
- 331 Oriented hyperlens based on passivated porous graphene phases for sub-diffraction visible imaging. **2021**, 11, 2839
- 330 Common workflows for computing material properties using different quantum engines. **2021**, 7, 4
- 329 Prediction of double-Weyl points in the iron-based superconductor $\text{CaKFe}_4\text{As}_4$. **2021**, 104, 0
- 328 Character of Doped Holes in $\text{Nd}_{1-x}\text{Sr}_x\text{NiO}_2$. **2021**, 6, 33 0
- 327 Gaussian Process Regression for Materials and Molecules. **2021**, 121, 10073-10141 66
- 326 Theoretical Study on the Contacting Interface-Dependent Band Alignments of $\text{CsPbBr}_3/\text{MoS}_2$ van der Waals Heterojunctions: Spin-Orbit Coupling Does Matter. 2
- 325 Superconductivity in Y_4RuGe_8 with a Vacancy-Ordered CeNiSi_2 -Type Superstructure. 1
- 324 Surface and subsurface damage in 14 MeV Au ion-irradiated diamond. **2021**, 130, 105303
- 323 Radioactive decay of ($\text{mathrm } \{{}^{\{90\}}\text{Sr}\}$) in cement: a non-equilibrium first-principles investigation. **2021**, 75, 1
- 322 Using general computational chemistry strategy to unravel the reactivity of emerging pollutants: An example of sulfonamide chlorination. **2021**, 202, 117391 3
- 321 NO reduction with CO over a highly dispersed Mn/TiO catalyst at low temperature: a combined experimental and theoretical study. **2021**, 32, 0
- 320 Reversible spin textures with giant spin splitting in two-dimensional GaXY (X=Se, Te; Y=Cl, Br, I) compounds for a persistent spin helix. **2021**, 104, 2
- 319 Computational methods for 2D materials modelling. **2021**, 84, 1
- 318 Atomic-scale study of Si-doped ALAs by cross-sectional scanning tunneling microscopy and density functional theory. **2021**, 104, 0

317	Density Functional Theory Study of Reaction Equilibria in Signal Amplification by Reversible Exchange. 2021 , 22, 1947-1957	2
316	Tribological behaviour of microalloyed Cu50Zr50 alloy. 1-22	
315	Thermal effect of epilayer on phonon transport of semiconducting heterostructure interfaces. 2021 , 178, 121613	2
314	Many-core acceleration of the first-principles all-electron quantum perturbation calculations. 2021 , 267, 108045	0
313	Emerging artificial intelligence in piezoelectric and triboelectric nanogenerators. 2021 , 88, 106227	21
312	Cold and hot uranium in DFT calculations: Investigation by the GTH pseudopotential, PAW, and APW + lo methods. 2021 , 199, 110665	1
311	Effect of the projector augmented wave potentials on the simulation of thermodynamic properties of vanadium. 2021 , 6, 068401	1
310	DFT insights into the migration of effective electrons towards O2 for OH formation over electron-rich sites on BiOBr (0 0 1) surface. 2021 , 567, 150828	1
309	Exploring the necessary complexity of interatomic potentials. 2021 , 200, 110752	2
308	Comparison of densities obtained with competing density functional molecular codes. 2021 , 397, 113649	1
307	Stability of the sc16 polymorph of GaAs. 2021 , 159, 110233	0
306	Radial and three-dimensional nonlocal pseudopotential calculations in gradient-corrected Kohn-Sham density functional theory based on higher-order finite element methods. 2021 , 386, 114094	0
305	Data Science, Machine Learning and Artificial Intelligence Applied to Metals and Alloys Research: Past, Present, and Future. 2022 , 609-621	0
304	High-pressure synthesis of Ba2RhO4, a rhodate analog of the layered perovskite Sr-ruthenate. 2021 , 5,	1
303	Single-layer polymeric tetraoxa[8]circulene modified by s-block metals: toward stable spin qubits and novel superconductors. 2021 , 13, 4799-4811	2
302	Wave functions, electronic localization, and bonding properties for correlated materials beyond the Kohn-Sham formalism. 2021 , 103,	2
301	Assessing the oxygen reduction reaction by a 2-electron mechanism on ceria surfaces. 2021 , 23, 18580-18587	1
300	Effect of Linker Distribution in the Photocatalytic Activity of Multivariate Mesoporous Crystals. 2021 , 143, 1798-1806	14

299	Photovoltaic Materials Design by Computational Studies: Metal Sulfides. 2020 , 123-138	2
298	An Ontology for the Materials Design Domain. 2020 , 212-227	4
297	Big Data-Driven Materials Science and Its FAIR Data Infrastructure. 2019 , 1-25	3
296	Big Data-Driven Materials Science and Its FAIR Data Infrastructure. 2020 , 49-73	12
295	Electronic Structure: Basic Theory and Practical Methods. 2020 ,	38
294	Rechargeable Alkali-Ion Battery Materials: Theory and Computation. 2020 , 120, 6977-7019	68
293	Instilling defect tolerance in new compounds. 2017 ,	156
292	Chapter 16: Molecular Chain Packing and Conformation in π -Conjugated Polymers from Solid-state NMR. 2019 , 363-386	2
291	Vapochromism induced by intermolecular electron transfer coupled with hydrogen-bond formation in zinc dithiolene complex. 2020 , 8, 14939-14947	4
290	Large scale and linear scaling DFT with the CONQUEST code. 2020 , 152, 164112	17
289	Equation of state of atomic solid hydrogen by stochastic many-body wave function methods. 2020 , 153, 204107	1
288	Band alignment of π (Al _x Ga _{1-x}) ₂ O ₃ alloys via atomic solid-state energy scale approach. 2020 , 10, 125321	3
287	f90wrap: an automated tool for constructing deep Python interfaces to modern Fortran codes. 2020 , 32, 305901	5
286	Lattice distortion inducing local antiferromagnetic behaviors in FeAl alloys. 2020 , 32, 465805	2
285	The pseudoatomic orbital basis: electronic accuracy and soft-mode distortions in ABO ₃ perovskites. 2020 , 2, 025002	2
284	Pentacene and tetracene molecules and films on H/Si(111): level alignment from hybrid density functional theory. 2020 , 2, 035002	6
283	In operando active learning of interatomic interaction during large-scale simulations. 2020 , 1, 045005	6
282	First-principles study of the nontrivial topological phase in chains of 3d transition metals. 2020 , 101,	3

281	Using forces to accelerate first-principles anharmonic vibrational calculations. 2017 , 1,	2
280	Combining electronic structure and many-body theory with large databases: A method for predicting the nature of 4f states in Ce compounds. 2017 , 1,	9
279	One-hundred-three compound band-structure benchmark of post-self-consistent spin-orbit coupling treatments in density functional theory. 2017 , 1,	52
278	Real-space pairwise electrostatic summation in a uniform neutralizing background. 2018 , 2,	2
277	Zirconia and hafnia polymorphs: Ground-state structural properties from diffusion Monte Carlo. 2018 , 2,	13
276	Material design of indium-based compounds: Possible candidates for charge, valence, and bond disproportionation and superconductivity. 2019 , 3,	6
275	Voltage-dependent reconstruction of layered Bi ₂ WO ₆ and Bi ₂ MoO ₆ photocatalysts and its influence on charge separation for water splitting. 2019 , 3,	7
274	Locality and computational reliability of linear response calculations for molecular systems. 2019 , 3,	2
273	Dielectric-dependent hybrid functionals for heterogeneous materials. 2019 , 3,	23
272	Cubic and tetragonal perovskites from the random phase approximation. 2019 , 3,	6
271	Spin wave excitations of magnetic metalorganic materials. 2020 , 4,	1
270	Phase stabilities of MgCO ₃ and MgCO ₃ -II studied by Raman spectroscopy, x-ray diffraction, and density functional theory calculations. 2020 , 4,	15
269	Comprehensive analysis of the influence of dispersion on group-14 rutile-type solids. 2020 , 4,	1
268	Comparative study of Minnesota functionals performance on ferroelectric BaTiO ₃ and PbTiO ₃ . 2020 , 4,	3
267	Multiscale analysis of dislocation loops and voids in tungsten. 2020 , 4,	3
266	Discovering hierarchies among intermetallic crystal structures. 2020 , 4,	4
265	Validating first-principles molecular dynamics calculations of oxide/water interfaces with x-ray reflectivity data. 2020 , 4,	5
264	Creating Weyl nodes and controlling their energy by magnetization rotation. 2019 , 1,	18

263	Sign switching of dimer correlations in SrCu ₂ (BO ₃) ₂ under hydrostatic pressure. 2020 , 2,	6
262	Electronic-structure calculations for nonisothermal warm dense matter. 2020 , 2,	3
261	Many-electron calculations of the phase stability of ZrO ₂ polymorphs. 2020 , 2,	4
260	The crystalline structure of SrRuO ₃ : Application of hybrid scheme to the density functionals revised for solids. 2017 , 57,	2
259	First-principles study of Ti-doped sapphire. I. Formation and optical transition properties of titanium pairs. 2021 , 104,	3
258	Observation of fractional edge excitations in nanographene spin chains. 2021 , 598, 287-292	21
257	Reproducibility of atomistic friction computer experiments: a molecular dynamics simulation study. 2021 , 47, 1509-1521	1
256	A review of the multiscale mechanics of silicon electrodes in high-capacity lithium-ion batteries. 2022 , 55, 063001	2
255	GaSeClO: A Molecular Compound with Very Strong SHG Effect. 2021 , 60, 15653-15658	3
254	Prevalence of pretransition disordering in the rutile-to-CaCl ₂ phase transition of GeO ₂ . 2021 , 104,	
253	Density Functional Theory Study of Reaction Equilibria in Signal Amplification by Reversible Exchange. 2021 , 22, 1937-1938	2
252	Spin-polarized electromagnetic and optical response of full-Heusler Co ₂ VZ (Z = Al, Be) alloys for spintronic application. 2021 , 136, 1	0
251	Periodic Trends behind the Stability of Metal Catalysts Supported on Graphene with Graphitic Nitrogen Defects. 2021 , 6, 28215-28228	0
250	Extreme-scale ab initio quantum raman spectra simulations on the leadership HPC system in China. 2021 ,	1
249	Accelerating all-electron ab initio simulation of raman spectra for biological systems. 2021 ,	0
248	Iron Oxides Applied to Catalysis. 2017 , 409-425	1
247	FlyClockbase: Importance of Biological Model Curation for Analyzing Variability in the Circadian Clock of <i>Drosophila melanogaster</i> by Integrating Time Series from 25 Years of Research.	
246	Density functional theory calculation of diffusion mechanism of intrinsic defects in rutile TiO ₂ . 2018 , 67, 176101	2

- 245 Encyclopedia of Big Data Technologies. **2019**, 358-365
- 244 Electronic Structure of Atomically Precise Graphene Nanoribbons. **2019**, 1-35
- 243 Theory and Models. **2019**, 69-76
- 242 Computational Thermodynamics: Application to Nuclear Materials. **2020**, 814-849
- 241 Pd NMR and NQR study of the cubic heavy fermion system CePdSi. **2020**, 32, 245601 0
- 240 The Dynamical Ensemble of the Posner Molecule Is Not Symmetric. **2021**, 12, 10372-10379 1
- 239 Surface Engineering of Flower-Like Ionic Liquid-Functionalized Graphene Anchoring Palladium Nanocrystals for a Boosted Ethanol Oxidation Reaction. **2021**, 60, 17388-17397 5
- 238 DFT studies on PbO₂ and binary PbO₂/SnO₂ thin films. **2021**, 136, 115037 1
- 237 Electronic Structure of Atomically Precise Graphene Nanoribbons. **2020**, 685-719
- 236 The Materials Project: Accelerating Materials Design Through Theory-Driven Data and Tools. **2020**, 1751-1784 0
- 235 Estimation of the charge state of Th implanted in SiO₂ in the different atomic environment. **2020**, 1686, 012064
- 234 Charge Properties of Thorium Implanted in Silicon Oxide. **2020**, 83, 1569-1574
- 233 Understanding the charge storage mechanism of supercapacitors: in situ/operando spectroscopic approaches and theoretical investigations. 13
- 232 A complete thermodynamic and kinetic catalogue of the defect chemistry of hematite α -Fe₂O₃, its cation diffusion, and sample donor dopants. **2021**, 23, 25518-25532 2
- 231 Ab Initio Simulations of Semiconductor Surfaces and Interfaces. **2020**, 119-153
- 230 Nanotechnology for Water and Wastewater Treatment Using Graphene Semiconductor Composite Materials. **2020**, 1-34 1
- 229 Pd-P antibonding interactions in APd₂P₂ (A=Ca and Sr) superconductors. **2020**, 4, 1
- 228 Experimental and theoretical comparison of Al²⁷, Li⁷, and C¹³ magic-angle-spinning NMR spectra for metal-atom clusters with rotational symmetry in their unit cells. **2020**, 4,

227	The crystal structures of Fe-bearing MgCO ₃ and -carbonates at 98 GPa from single-crystal X-ray diffraction using synchrotron radiation. 2020 , 76, 715-719	3
226	All-electron real-time and imaginary-time time-dependent density functional theory within a numeric atom-centered basis function framework. 2021 , 155, 154801	3
225	Inq, a Modern GPU-Accelerated Computational Framework for (Time-Dependent) Density Functional Theory. 2021 ,	1
224	Ab initio investigation of topological phase transitions induced by pressure in trilayer van der Waals structures: the example of h-BN/SnTe/h-BN. 2021 , 33, 025003	0
223	Origins of the transformability of nickel-titanium shape memory alloys. 2020 , 4,	1
222	Pressure-induced Pb-Pb bonding and phase transition in PbSnO. 2020 , 76, 979-991	4
221	Molecular dynamics simulation for hydrogen recycling on tungsten divertor for neutral transport analysis. 2021 , 60, SAAB08	
220	First-principles adaptive-boost accelerated molecular dynamics simulation with effective boost potential construction methods: a study of Li diffusion in Si crystal. 2020 , 59, 125002	
219	Design of Materials for Nuclear Energy Applications: First-Principles Calculations and Artificial Intelligence Methods. 2020 , 58, 907-937	0
218	Tests on the Accuracy and Scalability of the Full-Potential DFT Method Based on Multiple Scattering Theory. 2020 , 8, 590047	
217	Assessment of the van der Waals, Hubbard U parameter and spin-orbit coupling corrections on the 2D/3D structures from metal gold congeners clusters. 2021 ,	0
216	Tunable bandgap and vacancy defects in GaSe/SnSe van der Waals heterostructure. 2021 , 36, 4927	
215	Adsorption of small organic acids and polyphenols on hematite surfaces: Density Functional Theory+thermodynamics analysis. 2021 , 609, 469-469	0
214	Acidity effect on benzene methylation kinetics over substituted H-MeAlPO-5 catalysts. 2021 ,	2
213	Theoretical characterization and computational discovery of ultra-wide-band-gap semiconductors with predictive atomistic calculations. 1	1
212	On the Elastic Tensors of Ultra-Thin Films: A Study of Ruthenium.	
211	A reentrant phase transition and a novel polymorph revealed in high-pressure investigations of CF up to 46.5 GPa.. 2022 , 156, 044503	0
210	Enhanced Vertical Conductivity in Few-layer Graphene and Graphite with Transition Metal Intercalation: a Theoretical Study. 2020 ,	

209	Effect of Doping on the Electronic Structure of the Earth's Lower Mantle Compounds: FeXO with X = C, Al, Si.. 2022 , 15,	
208	Dispersion interactions in proposed covalent superhydride superconductors. 2022 , 105,	0
207	Metal-insulator transition and local-moment collapse in negative charge transfer CaFeO ₃ under pressure. 2022 , 105,	0
206	Development of a Metal-Organic Framework/Textile Composite for the Rapid Degradation and Sensitive Detection of the Nerve Agent VX. 2022 , 34, 1269-1277	5
205	Thermal excitation signals in the inhomogeneous warm dense electron gas.. 2022 , 12, 1093	4
204	Full versus quasiparticle self-consistency in vertex-corrected GW approaches. 2022 , 105,	0
203	Autonomous Design of Photoferroic Ruddlesden-Popper Perovskites for Water Splitting Devices.. 2022 , 15,	1
202	Determining the Adsorption Energetics of 2,3-Butanediol on RuO ₂ (110): Coupling First-Principles Calculations With Global Optimizers. 2022 , 9,	
201	Novel Calcium sp ³ Carbonate CaC ₂ O ₅ -I4 2d May Be a Carbon Host in Earth's Lower Mantle. 2022 , 6, 73-80	2
200	Theoretical insights into effective electron transfer and migration behavior for CO reduction on the BiOBr(001) surfaces.. 2022 ,	0
199	Cubic Crystal Structure Formation and Optical Properties within the Ag-B-M-X (B = Sr, Pb; M = Si, Ge, Sn; X = S, Se) Family of Semiconductors.. 2022 , 61, 2929-2944	0
198	Okra-like hollow Cu _{0.15} -CoP/Co ₃ O ₄ @CC nanotube arrays catalyst for overall water splitting. 2022 , 47, 7168-7179	0
197	Antioxidant Triggered Metallic 1T' Phase Transformations of Chemically Exfoliated Tungsten Disulfide (WS ₂) Nanosheets.. 2022 , e2107557	0
196	Pair structure, diffusion and pressure in liquid CuZr alloys from ab initio simulations: assessing the sensitivity to the energy cutoff.	
195	Modeling of Ferroelectric Oxide Perovskites: From First to Second Principles. 2022 , 13,	2
194	Density Functional Theory for Transition Metal Catalysis. 2022 ,	
193	Impact of alkaline-earth doping on electronic properties of the photovoltaic perovskite CsSnI ₃ : insights from a DFT perspective.. 2022 ,	
192	On the influence of water on THz vibrational spectral features of molecular crystals.. 2022 ,	1

191	Effect of Amino Acids on the Oxidation of Pyrite: Insights from Electrochemistry and Theoretical Dft Calculation.	
190	Tuning the dielectric response in a nanocomposite material through nanoparticle morphology.. 2022 , 12, 10778-10787	0
189	Edge-sharing BO ₄ tetrahedra and penta-coordinated silicon in the high-pressure modification of NaBSi ₃ O ₈ .	0
188	From Raman Mechanochemistry to "NMR Crystallography": Understanding the Structures and Interconversion of Zn-Terephthalate Networks Using Selective O-Labeling.. 2022 , 34, 2292-2312	2
187	Giant magnetoresistance, Fermi-surface topology, Shoenberg effect, and vanishing quantum oscillations in the type-II Dirac semimetal candidates MoSi ₂ and WSi ₂ . 2022 , 105,	1
186	High-pressure Na ₃ (N ₂) ₄ , Ca ₃ (. 2022 , 6,	0
185	Accuracy and Precision in Electronic Structure Computation: Wien2k and FPLO. 2022 , 10, 28	0
184	CeTaN ₃ and CeNbN ₃ : Prospective Nitride Perovskites with Optimal Photovoltaic Band Gaps. 2022 , 34, 2107-2122	2
183	Deposition, Characterization, and Performance of Spinel InGaZnO ₄ . 2022 , 4, 1238-1249	2
182	High-Pressure Synthesis of Superconducting SnS Using a Diamond Anvil Cell with a Boron-Doped Diamond Heater.. 2022 ,	
181	Fe ³⁺ -hosting carbon phases in the deep Earth. 2022 , 105,	0
180	Structure Evolution of Graphitic Surface upon Oxidation: Insights by Scanning Tunneling Microscopy.. 2022 , 2, 723-730	1
179	Molecular Property Prediction and Molecular Design Using a Supervised Grammar Variational Autoencoder.. 2022 ,	1
178	Electronic, Structural, and Mechanical Properties of SiO ₂ Glass at High Pressure Inferred from its Refractive Index.. 2022 , 128, 077403	2
177	Roadmap on Machine Learning in Electronic Structure.	7
176	On-surface synthesis of porous graphene nanoribbons containing nonplanar [14]annulene pores.	1
175	MARMOT: magnetism, anisotropy, and more, using the relativistic disordered local moment picture at finite temperature. 2022 , 4, 017001	0
174	Molecular Magnetism. 2022 , 52,	4

173	Phase stability of the argon crystal: first-principles study based on random phase approximation plus renormalized single excitation corrections. 2022 , 24, 033049	1
172	Free and open source software for computational chemistry education.	1
171	Mercury goes Solid at room temperature at nanoscale and a potential Hg waste storage.. 2022 , 12, 3494	
170	Fast All-Electron Hybrid Functionals and Their Application to Rare-Earth Iron Garnets. 2022 , 9,	
169	Band Structure of Organic-Ion-Intercalated (EMIM)FeSe Superconductor.. 2022 , 15,	
168	Elucidating the Role of B-Site Cations toward CO ₂ Reduction in Perovskite-Based Solid Oxide Electrolysis Cells. 2022 , 169, 034532	1
167	First-principles investigation of CZTS Raman spectra. 2022 , 6,	
166	On the elastic tensors of ultra-thin films: A study of ruthenium. 2022 , 153194	0
165	NiMo@C ₃ N ₅ heterostructures with multiple electronic transmission channels for highly efficient hydrogen evolution from alkaline electrolytes and seawater. 2022 , 438, 135379	6
164	Conferring all-nitrogen aromatics extra stability by acidic trapping. 2022 , 355, 118939	
163	Detecting a Hierarchy of Deep-Level Defects in the Model Semiconductor ZnSiN ₂ . 2021 , 125, 27959-27965	1
162	Tuning the quasi-harmonic treatment of crystalline ionic liquids within the density functional theory.. 2021 ,	0
161	Unexpected Electron Transport Suppression in a Heterostructured Graphene-MoS Multiple Field-Effect Transistor Architecture.. 2021 ,	0
160	Charge-spin interconversion in graphene-based systems from density functional theory. 2021 , 104,	1
159	Distinguishing between Similar Mini-proteins with Single-Molecule Nanopore Sensing: A Computational Study.	1
158	Proton-electron-coupled functionalities of conductivity, magnetism, and optical properties in molecular crystals.. 2022 ,	1
157	Numerical quality control for DFT-based materials databases. 2022 , 8,	1
156	Bond formation at polycarbonate X interfaces (X = Ti, Al, TiAl) probed by X-ray photoelectron spectroscopy and density functional theory molecular dynamics simulations. 2022 , 153363	

155	Maximizing the electronic charge carriers in donor-doped hematite under oxygen-rich conditions via doping and co-doping strategies revealed by density functional theory calculations. 2022 , 131, 155705	3
154	The Magnetic Genome of Two-Dimensional van der Waals Materials.. 2022 ,	10
153	Self-Assembly Silver Nanoparticles Decorated on Gold Nanoislands for Label-Free Localized Surface Plasmon Resonance Biosensing. 2200339	0
152	First-principles derivation and properties of density-functional average-atom models. 2022 , 4,	2
151	Table_1.DOCX. 2020 ,	
150	Band-filling effects in single-crystalline oligomer models for doped PEDOT: 3,4-ethylenedioxythiophene (EDOT) dimer salt with hydrogen-bonded infinite sulfate anion chains.	
149	Toward graphene-based devices for nanospintronics. 2022 , 249-274	
148	Designing 3d metal oxides: selecting optimal density functionals for strongly correlated materials.. 2022 ,	0
147	Computational Techniques for Nanostructured Materials. 2022 , 1-22	
146	Near Room-Temperature Synthesis of Vertical Graphene Nanowalls on Dielectrics.. 2022 ,	0
145	FAIR data enabling new horizons for materials research.. 2022 , 604, 635-642	6
144	Is There a Polaron Signature in Angle-Resolved Photoemission of CsPbBr ₃ ?. 2022 , 128, 176405	0
143	DFT investigations of AgMCHN (M = Cl, Br, and I) metal organic molecules: NMR, optoelectronic, and transport properties.. 2022 , 28, 136	0
142	Thermodynamic Re-assessment of the Nb-Zr System Using the CE \bar{V} M Model for Solid Solution Phases. 1	
141	Structural and electronic properties of the random alloy ZnSexS1 $\bar{4}$. 2022 , 105,	
140	Intrinsically High Magnetic Performance in Core-shell Structural (Sm, Y)Fe -based Permanent Magnets.. 2022 , e2203503	2
139	First principles study on structure and mechanical properties of Cr ₂ AlC. 2022 , 12, 055019	
138	Molecular simulation investigations on the coating of Al-alloy surface by nano-SiO ₂ -epoxy composite. 2022 ,	

137	Powder metallurgical 3D nickel current collectors with plasma-induced Ni ₃ N nanocoatings enabling long-life and dendrite-free lithium metal anode. 2022 ,	4
136	Unusual Ordering Behavior of Co ₃ Al-Based η Phase with L12 Structure Predicted by the Thermodynamic Model with Support of First-Principles Calculations.	
135	Atomistic Assessment of Melting Point Depression and Enhanced Interfacial Diffusion of Cu in Confinement with AlN.	0
134	Lattice dynamics and elastic properties of black phosphorus. 2022 , 105,	0
133	A DFT study of ZnO, Al ₂ O ₃ and SiO ₂ ; combining X-ray spectroscopy, chemical bonding and Wannier functions. 2022 , 110788	0
132	Donors, Acceptors, and a Bit of Aromatics: Electronic Interactions of Molecular Adsorbates on hBN and MoS ₂ Monolayers.	0
131	Ehrenfest dynamics implemented in the all-electron package exciting.	1
130	Synthesizing AlN Coatings Using Suspension Plasma Spraying: Effect of Promotional Additives and Aluminum Powder Particle Size.	1
129	Molecular Arrangement Control of [1]Benzothieno[3,2-b][1]benzothiophene (BTBT) via Charge-Assisted Hydrogen Bond.	1
128	Hybrid Kohn-Sham+Thomas-Fermi scheme for high-temperature density functional theory. 2022 , 105,	0
127	New Alkaline-Earth Amidosulfates and their Unexpected Decomposition to S ₄ N ₄ .	0
126	Elucidating CO Oxidation Pathways on Rh Atoms and Clusters on the $\sqrt{9}\times\sqrt{9}$ Cu ₂ O/Cu(111) Surface. 2022 , 126, 11091-11102	0
125	Two-gap superconductivity in a Janus MoSH monolayer. 2022 , 105,	2
124	Atomic engineering promoted electrooxidation kinetics of manganese-based cathode for stable aqueous zinc-ion batteries.	3
123	Giant Manipulation of Phonon Hydrodynamics in Ferroelectric Bilayer Boron Nitride at Room Temperature and Beyond.	0
122	Favorable Bonding and Band Structures of Cu ₂ ZnSnS ₄ and CdS Films and Their Photovoltaic Interfaces.	1
121	Ephemeral data derived potentials for random structure search. 2022 , 106,	2
120	Identifying Redox Orbitals and Defects in Lithium-Ion Cathodes with Compton Scattering and Positron Annihilation Spectroscopies: A Review. 2022 , 7, 47	0

- 119 Magnetism between magnetic adatoms on monolayer NbSe₂.
- 118 Machine Learning for Electrocatalyst and Photocatalyst Design and Discovery. 5
- 117 The Study of Metal Carbonyl Complexes by Means of Computational IR Spectra Analysis: A Remote Didactic Approach Based on Chemical Thinking. 0
- 116 Effects of thermal, elastic, and surface properties on the stability of SiC polytypes. **2022**, 106, 1
- 115 Graphene as an Adsorption Template for Studying Double Bond Activation in Catalysis. **2022**, 126, 14116-14124
- 114 Electronic and structural properties of crystalline and amorphous (TaNbHfTiZr)C from first principles. **2022**, 34, 425403
- 113 Understanding the Photoelectrochemical Properties of Theoretically Predicted Water-Splitting Catalysts for Effective Materials Discovery. 2201869
- 112 Beyond GGA total energies for solids and surfaces. **2022**, 157, 050401
- 111 Interaction of CO₂ with TiO₂/reduced graphene oxide as superior catalysts: Dispersion-corrected density functional theory simulation. **2022**, 128, 109279
- 110 Intrinsic coercivity in 4f-3d intermetallic magnets with valence fluctuations. **2022**, 562, 169748
- 109 Simulating key properties of lithium-ion batteries with a fault-tolerant quantum computer. **2022**, 106, 1
- 108 A comprehensive investigation of structural and magnetic phase stability, electronic, magnetic and thermoelectric properties of Co₂FeZ (Z = Al, Ga, Si, Ge, S, Se and Te) Full Heusler alloys. **2022**, 355, 114947 0
- 107 The site preference and doping effect on mechanical properties of Ni₃Al-based η phase in superalloys by combing first-principles calculations and thermodynamic model. **2022**, 15, 104278 0
- 106 The ordering behavior of Co₃Al-based η phase with L1₂ structure predicted by the thermodynamic model with support of first-principles calculations. **2022**, 33, 104447 0
- 105 Machine learning for high-entropy alloys: Progress, challenges and opportunities. **2023**, 131, 101018 1
- 104 Compound-tunable embedding potential method: analysis of pseudopotentials for Yb in YbF₂, YbF₃, YbCl₂ and YbCl₃ crystals. **2022**, 24, 19333-19345 0
- 103 Elucidation of the atomic-scale processes of dissociative adsorption and spillover of hydrogen on the single atom alloy catalyst Pd/Cu(111). **2022**, 24, 21705-21713 0
- 102 Thermoelectric, spin-dependent optical and quantum transport properties of 2D half-metallic Co₂Se₃. **2022**, 24, 22016-22027 0


- 101 A two-dimensional Be₂Au monolayer with planar hexacoordinate s-block metal atoms: a superconducting global minimum Dirac material with two perfect Dirac node-loops. **2022**, 13, 11099-11109 ○
- 100 DFT Exchange: Sharing Perspectives on the Workhorse of Quantum Chemistry and Materials Science. 9
- 99 Reproducibility of Hybrid Density Functional Calculations for Equation-of-State Properties and Band Gaps. **2022**, 126, 5924-5931 ○
- 98 Modeling Short-Range Ordering in Binary BCC Ti-X (X = Nb, V, Zr) Alloys using CE-CVM. **2022**, 43, 511-526 ○
- 97 Ion Conductivity in a Magnesium Borohydride Ammonia Borane Solid-State Electrolyte. **2022**, 126, 15118-15127 ○
- 96 Accurately Determining the Phase Transition Temperature of CsPbI₃ via Random-Phase Approximation Calculations and Phase-Transferable Machine Learning Potentials. ○
- 95 Similarity of materials and data-quality assessment by fingerprinting. ○
- 94 Spinor GW /Bethe-Salpeter calculations in BerkeleyGW: Implementation, symmetries, benchmarking, and performance. **2022**, 106, 1
- 93 Digital Twin Assistant Active Design and Optimization of Steel Mega-Sub Controlled Structural System under Severe Earthquake Waves. **2022**, 15, 6382 ○
- 92 Zero-point renormalization of the band gap of semiconductors and insulators using the projector augmented wave method. **2022**, 106, ○
- 91 Dynamic bonding influenced by the proximity of adatoms to one atom high step edges. **2022**, 106, ○
- 90 Effect of Nitrogen Doping and Oxidation of Graphene on the Deposition of Platinum from Trimethyl(methylcyclopentadienyl)platinum(IV). **2022**, 126, 16357-16368 ○
- 89 Theoretical investigation of high coverage water adsorption on Co and Ni doped Al₂O₃ surface. **2022**, 57, 16710-16724 ○
- 88 Heisenberg's uncertainty principle in the PTOLEMY project: A theory update. **2022**, 106, ○
- 87 Adaptively compressed exchange in the linearized augmented plane wave formalism. **2022**, 106, ○
- 86 Intrinsic glassy-metallic transport in an amorphous coordination polymer. 1
- 85 Electronic and Optical Properties of III-V Binary 2D Semiconductors: How to Achieve High Precision from Accurate Many-Body Methods. ○
- 84 Computational Techniques for Nanostructured Materials. **2022**, 459-480 ○

- 83 Complex amorphous oxides: property prediction from high throughput DFT and AI for new material search. ○
- 82 Electrically modulated reversible dual-spin filter in zigzag SiC7 nanoribbons. **2022**, 24, 25656-25662 ○
- 81 Chemical Bonding With Plane Waves. **2022**, ○
- 80 Challenges in the modelling of elementary steps in electrocatalysis. **2022**, 101170 ○
- 79 Theoretical Modeling of High Spin to Low Spin Transition and Structural Stability Under Pressure in CaFeO₃. ○
- 78 Wigner Formulation of Thermal Transport in Solids. **2022**, 12, ○
- 77 Electronic structure of Bi nanolines on InAs(100). **2022**, 155436 ○
- 76 First-principles equation of state of CHON resin for inertial confinement fusion applications. **2022**, 106, ○
- 75 Computational design of magnetic molecules and their environment using quantum chemistry, machine learning and multiscale simulations. 2
- 74 Band gaps of halide perovskites from a Wannier-localized optimally tuned screened range-separated hybrid functional. **2022**, 6, 1
- 73 Piezoelectric ferromagnetism in two-dimensional materials via materials screening. **2022**, 106, ○
- 72 Approaching the basis-set limit of the dRPA correlation energy with explicitly correlated and projector augmented-wave methods. ○
- 71 Variationally consistent Hellmann-Heynman forces in the finite element formulation of Kohn-Sham density functional theory. **2023**, 403, 115674 ○
- 70 FAIR Big Data in the Materials Design Domain. **2022**, 1-8 ○
- 69 Fathoming the anisotropic magnetoelasticity and magnetocaloric effect in GdNi. **2022**, 106, ○
- 68 Structural and electronic evidence of boron atomic chains. **2022**, 106, 1
- 67 Soft and transferable pseudopotentials from multi-objective optimization. **2022**, 108594 1
- 66 Vacancy-Driven Disorder and Elevated Dielectric Response in the Pyrochlore Pb_{1.5}Nb₂O_{6.5}. ○

- 65 Quasi-One-Dimensional Linarite-Type $\text{PbCu}(\text{SeO}_4)(\text{OH})_2$ with Competing Nearest-Neighbor and Next-Nearest-Neighbor Intrachain Exchange Interactions. **2022**, 15, 7860 ○
- 64 Parallel-Self-Assembling Stack, Center-Capture Effect, and Reactivity-Enhancing Effect of N-Layer ($N = 1, 2, 3$) Cyclo[18]carbon. ○
- 63 Reversible canted persistent spin textures in two-dimensional ferroelectric bilayer WTe_2 . **2022**, 132, 183906 ○
- 62 Neutral Radical Molecular Conductors Based on a Gold Dimethoxybenzenedithiolene Complex with and without Crystal Solvent. ○
- 61 Rich magnetic phase transitions and completely dual-spin polarization of zigzag PC3 nanoribbons under uniaxial strain. ○
- 60 CASM \square software package for first-principles based study of multicomponent crystalline solids. **2023**, 217, 111897 ○
- 59 Two-dimensional Be_2Al and Be_2Ga monolayer: anti-van Hove/Le Bel planar hexacoordinate bonding and superconductivity. ○
- 58 Fundamentals and advances of ligand field theory in understanding structure-electrochemical property relationship of intercalation-type electrode materials for rechargeable batteries. **2023**, 133, 101055 2
- 57 Exchange-Correlation Functional Comparison of Electronic Energies in Atoms Using a Grid Basis. **2022**, 10, 3392-3407 ○
- 56 Ab initio methods for the computation of physical properties and performance parameters of electrochemical energy storage devices. ○
- 55 A universal graph deep learning interatomic potential for the periodic table. **2022**, 2, 718-728 ○
- 54 Effects of Vacancy Defects on Electrical and Optical Properties of ZnO/WSe_2 Heterostructure: First-Principles Study. **2022**, 12, 1975 ○
- 53 Classical and machine learning interatomic potentials for BCC vanadium. **2022**, 6, ○
- 52 Influence of germanium substitution on the structural and electronic stability of the competing vanadium dioxide phases. **2022**, 4, ○
- 51 Comparing the accuracy of melting temperature prediction methods for high entropy alloys. **2022**, 132, 205901 ○
- 50 Exploiting Machine Learning in Multiscale Modelling of Materials. ○
- 49 Na_7RbTl_4 \square A New Ternary Zintl Phase Containing $[\text{Tl}_4]^{8-}$ Tetrahedra. **2022**, 648, ○
- 48 Superexchange and spin-orbit coupling in monolayer and bilayer chromium trihalides. **2022**, 106, ○

- 47 New Insights into the Volume Isotope Effect of Ice Ih from Polarizable Many-Body Potentials. **2022**, 13, 11831-11836
- 46 Boosted Output Voltage of BiSbTe-Based Thermoelectric Generators via Coupled Effect between Thermoelectric Carriers and Triboelectric Charges. 2202987
- 45 Steering on-surface reactions through molecular steric hindrance and molecule-substrate van der Waals interactions. **2022**, 1,
- 44 Hybrid Finite Element/Multipole Expansion Method for Atomic Kohn-Sham Density Functional Theory Calculations. **2023**, 108658
- 43 Strain dependence of the thermoelectric properties of perovskite MgSiO₃: A first principles study. **2023**, 133, 025101
- 42 Highly efficient perovskite solar cells by building 2D/3D perovskite heterojunction in situ for interfacial passivation and energy level adjustment.
- 41 Superconductivity of graphenelike hydrogen in H₂He at high pressure. **2023**, 107,
- 40 Methods of Modeling of Strongly Correlated Electron Systems. **2023**, 13, 238
- 39 Nonlinear elastic behavior of 2D materials using molecular statics and comparisons with first principles calculations. **2023**, 148, 115633
- 38 Material normal energy distribution for field emission analyses from monocrystalline surfaces. **2023**, 2420, 012033
- 37 Multicomponent solid solution with pyrochlore structure. **2023**,
- 36 Step Structures and Adatom Diffusion on SiC Surfaces. **2023**, 66, 239-244
- 35 Assessing Factors that Determine Adatom Migration and Clustering on a Thin Film Oxide; Pt₁ and Rh₁ on the $\sqrt{3}\times\sqrt{3}$ Cu₂O/Cu(111) Surface. **2023**, 157145
- 34 New Strategy to Improve Photocatalytic Activity and Mechanistic Aspect for Water Splitting.
- 33 Hyperfine properties at Zr sites of Zr-based compounds. A DFT FP-LAPW and GIPAW study. **2023**, 657, 414757
- 32 Equilibrium fractionation of REE isotopes in nature: Insights from NRIXS and DFT+U studies of Eu and Dy phonon density of states. **2023**, 348, 323-339
- 31 Small-data-based machine learning interatomic potentials for graphene grain boundaries enabled by structural unit model. **2023**, 11, 100260
- 30 Theoretical Calculations on Metal Catalysts Toward Water-Gas Shift Reaction: a Review.

- 29 All-Electron Plane-Wave Electronic Structure Calculations. **2023**, 19, 1300-1309 ○
- 28 Inducing Fe 3d Electron Delocalization and Spin-State Transition of FeN₄ Species Boosts Oxygen Reduction Reaction for Wearable Zinc-Air Battery. **2023**, 15, ○
- 27 Vibrational and electronic properties of Na₂Ti₆O₁₃. ○
- 26 Zwitterionic or Not? Fast and Reliable Structure Determination by Combining Crystal Structure Prediction and Solid-State NMR. **2023**, 28, 1876 ○
- 25 Massively parallel fitting of Gaussian approximation potentials. **2023**, 4, 015020 ○
- 24 Study of the Bandgap and Crystal Structure of Cu₄TiSe₄: Theory vs. Experiment. **2023**, 13, 331 ○
- 23 First-principles theoretical analysis of magnetically tunable topological semimetallic states in antiferromagnetic DyPdBi. **2023**, 107, ○
- 22 Electronic, Optical, Mechanical, and Electronic Transport Properties of SrCu₂O₂: A First-Principles Study. **2023**, 16, 1829 ○
- 21 Phase formation of powders sputtered from X₂BC targets and XC+XB powder mixtures {X = Nb, Ta, W}. **2023**, 458, 129379 ○
- 20 Structure evolution and mechanical properties of Al-alloyed tantalum diboride films prepared by magnetron sputtering co-deposition. **2023**, 41, 023410 ○
- 19 Unravelling catalytic activity trends in ceria surfaces toward the oxygen reduction and water oxidation reactions. ○
- 18 A novel two-dimensional superconducting Ti layer: density functional theory and electron-beam irradiation. ○
- 17 The study of electronic structure and optical properties of Ba₂MnWO₆ within density functional theory. **2023**, 49, 274-281 ○
- 16 Band Gap Narrowing in a High-Entropy Spinel Oxide Semiconductor for Enhanced Oxygen Evolution Catalysis. **2023**, 145, 6753-6761 ○
- 15 Density functional theory. **2022**, ○
- 14 Signatures of Electric Field and Layer Separation Effects on the Spin-Valley Physics of MoSe₂/WSe₂ Heterobilayers: From Energy Bands to Dipolar Excitons. **2023**, 13, 1187 ○
- 13 Cathodoluminescence studies of point defects in aluminum nitride. **2023**, 13, 035133 ○
- 12 Evaluating the harmonic approximation for the prediction of thermodynamic formation properties of solids. **2023**, 223, 112152 ○

- 11 Optimized 2D nanostructures for catalysis of hydrogen evolution reactions. ○
- 10 Second-harmonic-generation of [(Se,Te)Cl₃]+[GaCl₄]⁻ with aligned ionic tetrahedra. ○
- 9 Enhanced Thermoelectric Performance of Tin(II) Sulfide Thin Films Prepared by Aerosol Assisted Chemical Vapor Deposition. ○
- 8 Meta-GGA SCAN Functional in the Prediction of Ground State Properties of Magnetic Materials: Review of the Current State. **2023**, 13, 728 ○
- 7 Magnetic Anisotropy of Single-ion Magnet (PPh₄)₂[ReF₆] · 2H₂O. ○
- 6 Computer simulations of the glass transition and glassy materials. **2023**, 24, 1-16 ○
- 5 Fabrication of MoS₂/Bi₂S₃ heterostructure for photocatalytic degradation of Metronidazole and Cefalexin and antibacterial applications under NIR light: experimental and theoretical approach. **2023**, 129, ○
- 4 Machine learning for perovskite solar cell design. **2023**, 226, 112215 ○
- 3 Semimetallic, Half-Metallic, Semiconducting, and Metallic States in Gd-Sb Compounds. **2023**, 24, 8778 ○
- 2  Ga₂O₃. ○
- 1 Proximity-enhanced valley Zeeman splitting at the WS₂/graphene interface. ○